JACS
JOURNAL OF THE AMERICAN CHEMICAL SOCIETY

Article

Investigations into the Mechanism of Inter- and Intramolecular Iron-Catalyzed [2+2] Cycloaddition of Alkenes

Matthew V. Joannou, Jordan M Hoyt, and Paul J. Chirik

J. Am. Chem. Soc., **Just Accepted Manuscript** • DOI: 10.1021/jacs.0c00250 • Publication Date (Web): 20 Feb 2020

is published by the American Chemical Society. 1155 Sixteenth Street N.W., Washington, DC 20036

Investigations into the Mechanism of Inter- and Intramolecular Iron-Catalyzed [2+2] Cycloaddition of Alkenes

Matthew V. Joannou, Jordan M. Hoyt, Paul J. Chirik*

Department of Chemistry, Princeton University, Princeton, New Jersey 08544, United States of America

ABSTRACT: Mechanistic studies are reported on the inter- and intramolecular [2+2] alkene cycloadditions to form cyclobutanes promoted by (^{tric}PDI)Fe(N_2) (^{tric}PDI = 2,6-(2,4,6-tricyclopentyl)C_6H_2N=CMe)$_2C_5H_3N$). A combination of kinetic measurements, freeze-quench ^{57}Fe Mössbauer and infrared spectroscopic measurements, deuterium labeling studies, natural abundance ^{13}C KIE studies, and isolation and characterization of catalytically relevant intermediates were used to gain insight into the mechanism of both inter- and intramolecular [2+2] cycloaddition reactions. For the stereo- and regioselective [2+2] cycloaddition of 1-octene to form *trans*-1,2-dihexylcyclobutane, a first-order dependence on both iron complex and alkene was measured as well as an inverse dependence on N_2 pressure. Both ^{57}Fe Mössbauer and infrared spectroscopic measurements identified (^{tric}PDI)Fe(N_2)(η^2-1-octene) as the catalyst resting state. Rate-determining association of 1-octene to (^{tric}PDI)Fe(η^2-1-octene) accounts for the first order dependence of alkene and the inverse dependence on N_2. Heavy atom ^{13}C/^{12}C kinetic isotope effects near unity also support post rate-determining C–C bond formation. By contrast, the intramolecular iron-catalyzed [2+2] cycloaddition of 1,7-octadiene yielded *cis*-bicyclo[4.2.0]octane in 92:8 d.r. and a first order dependence on the iron precursor and zeroth order behavior in both diene and N_2 pressure were measured. A pyridine(diimine) iron *trans*-bimetallacycle was identified as the catalyst resting state and was isolated and characterized by X-ray diffraction, ^{1}H NMR and ^{57}Fe Mössbauer spectroscopies. Dissolution of the iron *trans*-bimetallacycle in benzene-d_6 produced predominantly the *cis*-cyclobutane product, establishing interconversion between the *trans* and *cis* metallacycles during the catalytic reaction and consistent with a Curtin-Hammett kinetic regime. A primary ^{13}C/^{12}C kinetic isotope effect of 1.022(4) was measured at 23 °C, consistent with rate-determining unimolecular reductive elimination to form the cyclobutane product. Despite complications from competing cyclometallation of chelate aryl substituents, deuterium labeling experiments were consistent with unimolecular C–C reductive elimination that occurred either by a concerted pathway or a radical rebound sequence that is faster than C–C bond rotation.

■ INTRODUCTION

The synthesis of strained carbocycles is a challenge in organic chemistry with a host of potential applications in polymers, pharmaceuticals, fine chemicals, and fragrances.[1] In particular, the structural rigidity and strain in cyclobutanes offer a range of possible applications and the development and understanding of new catalytic processes for their synthesis is highly desirable to the synthetic community. Traditional routes to cyclobutanes from olefins employ radical- and photochemical-based methods designed to overcome the orbital symmetry constraints of thermally forbidden cycloadditions.[2] The substrates required for these reactions, however, are highly activated (α,β-unsaturated esters, allenes, etc.) and as a consequence can limit the scope and applicability of the transformation. The transition metal-catalyzed formal [2+2] cycloadditions of unactivated feedstock α-olefins have emerged as an attractive, atom-economical route to these valuable 4-membered rings.[3] A distinct advantage over radical-based processes is the opportunity for catalyst control, enabling the rational modification of chemo- and regioselectivity resulting in the precision synthesis of a variety of cyclic products.

Scheme 1. Previously reported pyridine(diimine) iron-catalyzed alkene-alkene and alkene-diene [2+2] cycloadditions, along with isolated and proposed metallacyclic intermediates. E = NR', CR'$_2$; *G* = alkyl, benzyl, heterobenzyl.

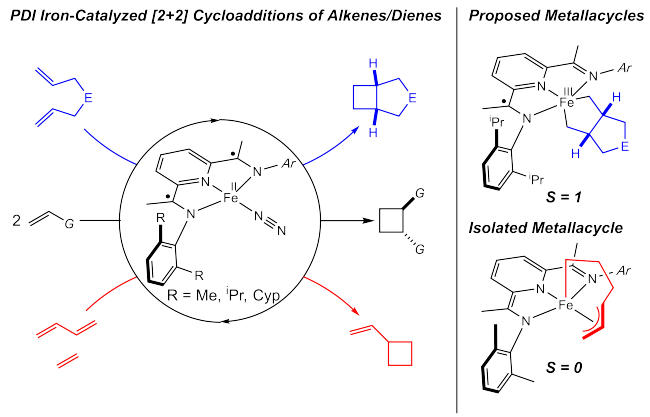

As presented in Scheme 1, our group has developed and studied several [2+2] cycloadditions of olefins to generate cyclobutanes, utilizing iron- and cobalt-catalysts bearing redox-active pyridine(diimine) (PDI) ligands.[4] For iron, both intra- and intermolecular reactions have been demonstrated in alkene-alkene and diene-alkene [2+2] cycloaddition reactions. While both combinations of coupling partners yielded 4-membered ring products, the observed organometallic intermediates formed during these reactions have different geometries, spin states and coordination numbers, raising

questions about the nature of the reductive elimination and C(sp^3)–C(sp^3) bond-forming step.

Previous studies on intramolecular alkene-alkene [2+2] cycloaddition resulted in isolation of catalytically competent S = 1 pyridine(diimine) iron bis(alkene) and metallacycle complexes (Scheme 1, right).[3] Structural, spectroscopic, and computational data supported the presence of the mono-reduced form of the chelate ([PDI]$^{1-}$) as the iron cycled between the two intermediates, consistent with an Fe(I)–Fe(III) redox cycle. For butadiene-ethylene coupling, an S = 0 pyridine(diimine) iron alkyl-allyl metallacycle was isolated and crystallographically characterized where the chelate is in its closed-shell dianionic form (Scheme 1, right).[4c] The isolated iron metallacycle did not undergo C–C reductive elimination at ambient temperature in solution, however upon addition of butadiene or carbon monoxide, vinyl cyclobutane was generated, consistent with "ligand-induced" reductive elimination.[4d]

Modification of the aryl groups on the pyridine(diimine) iron dinitrogen complex enabled the highly chemo-, regio- and diastereoselective intermolecular cycloaddition of unactivated alkenes. In contrast to the intramolecular cases where *cis* stereochemistry was observed, the intermolecular [2+2] cycloaddition of unactivated terminal alkenes promoted by **(^{tric}PDI)Fe(N$_2$)** (^{tric}PDI = 2,6-(2,4,6-tricyclopentyl)C$_6$H$_2$N=CMe)$_2$C$_5$H$_3$N) produced exclusively 1,2-*trans* products (Scheme 1, left).[4c] The cyclopentyl-subtituted aryl variant of the pyridine(diimine) ligand was used to suppress transfer hydrogenation of the alkene observed previously with the isopropyl variant, (^{iPr}PDI)Fe(N$_2$)$_2$, arising from cyclometallation of the aryl substituents.[4c] Aside from these phenomenological observations, little is known about the mechanistic details including the nature of the active species, catalyst deactivation pathways, and turnover-limiting step of these unique cycloaddition reactions. Ultimately such information will inform design of next generation catalysts with broader scope, lifetime, and activity. Here we describe a comprehensive mechanistic study into iron-catalyzed inter- and intramolecular [2+2] cycloadditions of unactivated alkenes (Scheme 2).

Scheme 2. Reactions investigated in this article and associated mechanistic questions.

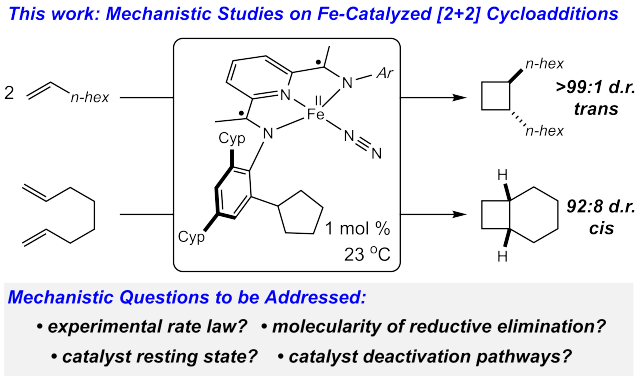

■ RESULTS AND DISCUSSION (INTERMOLECULAR)

Kinetic Studies. Our investigations commenced with studies into the iron-catalyzed [2+2] cycloaddition of 1-octene as a representative alkene. In addition to being a readily available α-olefin, 1-octene also has several advantageous physical properties including a mid-range boiling point of 122 °C that allows for facile separation of product from the starting material, as well as reliable kinetic measurements by analysis of reaction aliquots. 1-Octene also has an accessible melting-point (-101 °C) and glass-transition at that melting point which aids in the preparation of samples for freeze-quench ^{57}Fe Mössbauer studies.[5,7] As depicted in Figure 1, with 1 mol % **(^{tric}PDI)Fe(N$_2$)** in neat 1-octene, *trans*-1,2-dihexylcyclobutane was formed in 31% yield in >99% selectivity. The density functional theory (DFT)-computed thermodynamic properties of the [2+2] reaction establish a near thermoneutral reaction under standard conditions (B3LYP level of theory, see Supporting Information for more computational details). While highly enthalpically driven ($\Delta H°$ = -14.4 kcal·mol^{-1}), the large entropic penalty of the reaction ($\Delta S°$ = -46.4 cal·mol^{-1}·K^{-1}) results in an overall $\Delta G°$ of -0.7 kcal·mol^{-1}.

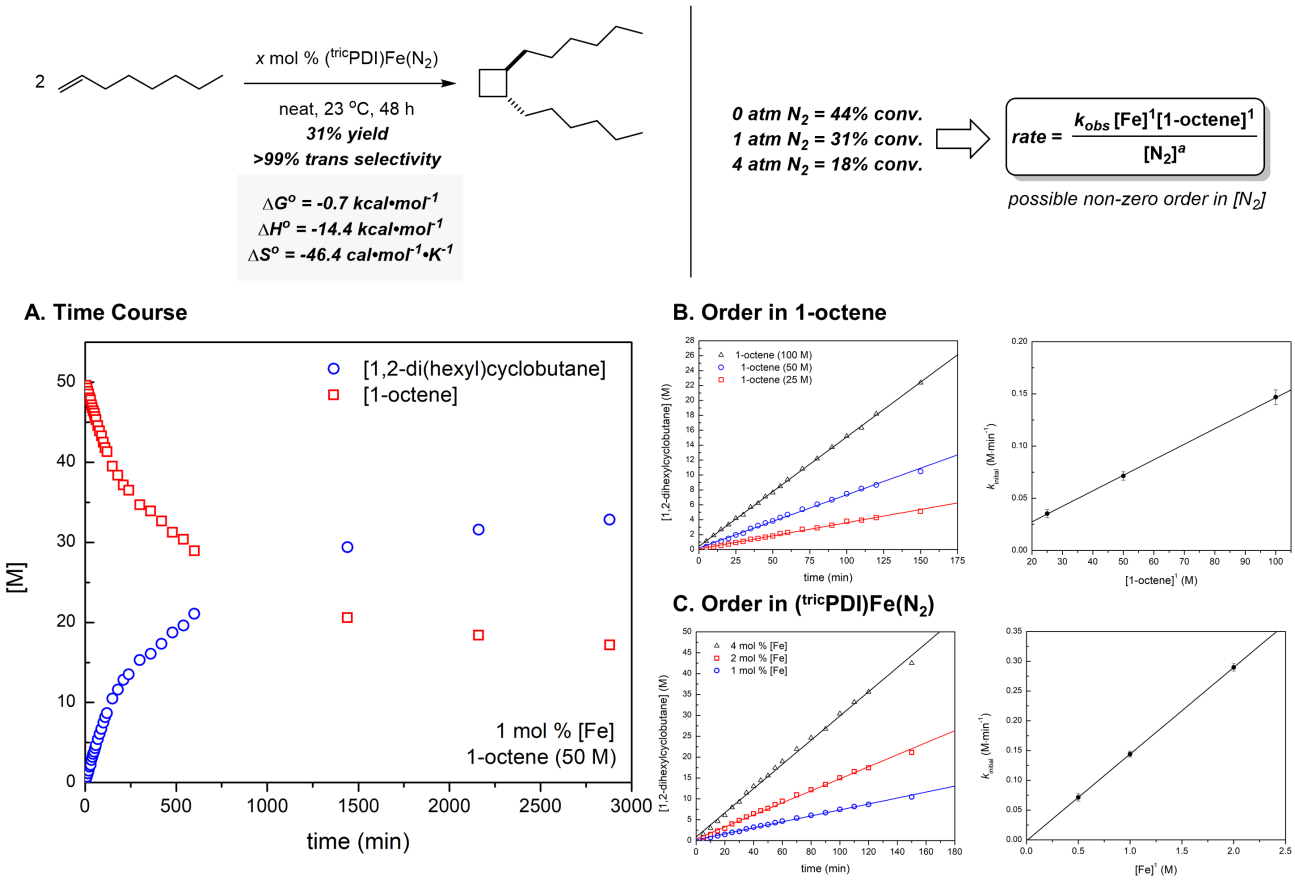

Figure 1. Kinetic analysis of iron-catalyzed [2+2] cycloaddition of 1-octene. A. Time course of the reaction from 0 to 48 hours. B. Initial rates plots for determining the order in 1-octene. C. Initial rates plots for determining the order in catalyst. 1 mol % Fe is equal to 0.5 M in **(tricPDI)Fe(N₂)**. *a* = unknown order, yet to be determined. "Yield" indicates isolated yield of the product, whereas "conversion" indicates conversion to product as determined by gas chromatography.

To determine the overall reaction order and rate-determining step, kinetic analysis on the cyclodimerization of 1-octene was performed. The progress of iron-catalyzed [2+2] cycloaddition of 1-octene ([**(tricPDI)Fe(N₂)**] = 0.5 M, [1-octene] = 50 M) was monitored by gas chromatography over the course of 48 hours at 23 °C. A representative reaction time course is presented in Figure 1A and establishes well-behaved kinetic behavior at early conversion with no induction period for the onset of catalysis. After approximately 20 turnovers, the rate of reaction begins to slow, leading to almost no catalysis after 24 hours, suggesting catalyst deactivation and ultimately death. Because of the well-behaved kinetics observed at early conversion, the order in iron catalyst and alkene were determined using the method of initial rates (Figure 1B, 1C). The data support a first order process in both the iron precatalyst and 1-octene for intermolecular iron-catalyzed [2+2] cycloaddition of alkenes.

Determination of Reaction Order in N₂. The presence of coordinated dinitrogen on the iron precatalyst suggested that removing it from the reaction may facilitate substrate coordination and improve overall catalytic performance. An inverse relationship between pressure and conversion to product after 48 hours of reaction was observed: 0 atm N_2 – 44% conv., 1 atm N_2 – 31% conv., 4 atm N_2 – 18% conv. (Figure 1, top). To determine whether N_2 pressure is a component of the Fe-catalyzed cyclodimerization rate law and to accurately assign its reaction order (i.e. the precise concentration of N_2 at the outset of any reaction), a more in-depth understanding of dinitrogen coordination properties of the iron precatalyst was required.

As has been reported previously,[8] PDI iron dinitrogen complexes often exist as equilibrium mixtures of mono- and bis-dinitrogen species in both solution and in the solid state (Figure 2A). A combination of ^{1}H NMR, infrared, and ^{57}Fe Mössbauer spectroscopies were used to determine the ratio of **(tricPDI)Fe(N₂)**:**(tricPDI)Fe(N₂)₂** under various conditions. Figure 2B presents the zero-field ^{57}Fe Mössbauer spectrum of **(tricPDI)Fe(N₂)ₙ** in the solid state at 80 K. The majority of the spectrum (90%) corresponds to a quadrupole doublet with an isomer shift (δ) of 0.39 mm/s and an absolute quadrupole splitting ($|\Delta E_Q|$) of 2.07 mm/s, while the minor doublet has parameters δ = 0.35 mm/s and $|\Delta E_Q|$ = 0.33 mm/s, corresponding to the bis-dinitrogen complex.[8] The spectroscopic data support the four-coordinate, iron mono-dinitrogen complex as the major compound in the solid state. The solid-state (KBr) infrared spectrum (Figure 2C, bottom) of **(tricPDI)Fe(N₂)ₙ** exhibits a strong band at 2036 cm^{-1}, assigned as the N–N stretch of the coordinated N_2 ligand of the four-coordinate complex. A second, less intense band at 2125 cm^{-1} was also observed and assigned as the antisymmetric stretch corresponding to **(tricPDI)Fe(N₂)₂**. The infrared data support the same ratio (90:10) of iron compounds as determined by ^{57}Fe Mössbauer spectroscopy at 1 atm of N_2. The ratio of four- to five-coordinate iron dinitrogen compounds was also studied in ben-

zene-d_6 solution at 1 atm of N_2. The solution infrared spectrum (Figure 2C, top) exhibits symmetric and anti-symmetric N_2 stretching bands for **(^{tric}PDI)Fe(N_2)$_2$** at 2125 and 2057 cm^{-1}, respectively. The broad line width of the band at 2057 cm^{-1} obscures the N_2 band for **(^{tric}PDI)Fe(N_2)** at 2038 cm^{-1}. From these data, at 1 atm N_2 in benzene at 23 °C a value of K_{eq} = 2.1 was established for the interconversion of the mono- and bis-dinitrogen compounds.[10] This ratio was further confirmed by NMR spectroscopy where the benzene-d_6 ^{1}H NMR spectrum of **(^{tric}PDI)Fe(N_2)$_n$** displayed broadened signals for the mono- and bis-dinitrogen complexes in a 1:2.1 ratio, respectively. Degassing a benzene-d_6 solution of **(^{tric}PDI)Fe(N_2)$_n$** leads to sharpening of the signals and >98% conversion to **(^{tric}PDI)Fe(N_2)**, as judged by ^{1}H NMR spectroscopy.

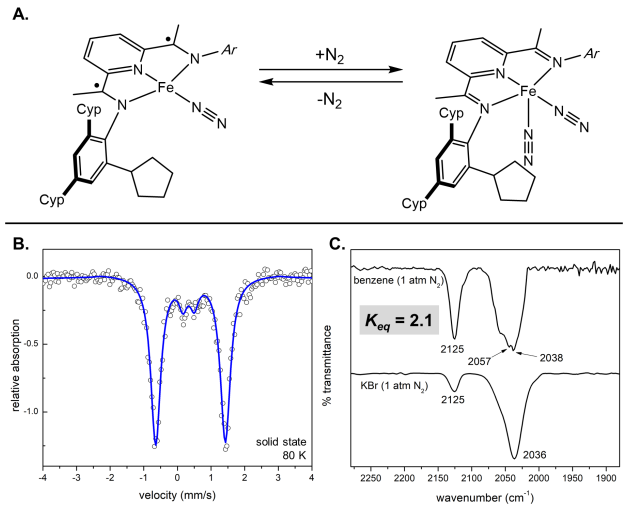

Figure 2. Determining the ratio of **(^{tric}PDI)Fe(N_2)**:**(^{tric}PDI)Fe(N_2)$_2$** in solution and in the solid state at 1 atm N_2. A. Equilibrium mixture of mono- and bis-dinitrogen complexes. B. Zero-field ^{57}Fe Mössbauer spectrum of **(^{tric}PDI)Fe(N_2)$_n$** at 80 K in the solid state. C. Stacked IR spectra of **(^{tric}PDI)Fe(N_2)$_n$** in benzene (top) and dispersed in a KBr pellet (bottom). Both samples were prepared at and spectra acquired at 23 °C and 1 atm N_2.

To avoid experimental complications from monitoring the [2+2] cycloaddition of 1-octene at different pressures of N_2, propylene was used as the alkene substrate as neat conditions were not required to obtained appreciable yields and the reaction was readily monitored by ^{1}H NMR spectroscopy over the course of 48 hours at 23 °C in benzene-d_6. Time courses for the reaction at both 0 and 1 atm of N_2 are presented in Figure 3A. As with 1-octene, the reaction displays well-behaved kinetic behavior at early conversion, followed by a decrease in rate as the reaction proceeds. Interestingly, while the initial rate of reaction at 0 atm N_2 is higher, the rate of catalyst deactivation increased without exogenous N_2, as both the 0 and 1 atm N_2 reactions reach the same conversion after 24 hours (71% conversion). This suggests that catalyst deactivation could involve N_2 displacement, rather than substrate inhibition (*vide infra*). Utilizing the method of initial rates (Figure 3B), the order in N_2 was determined to be -1 overall, corroborating the inverse relationship between conversion and N_2 pressure observed in the [2+2] cycloaddition of 1-octene.

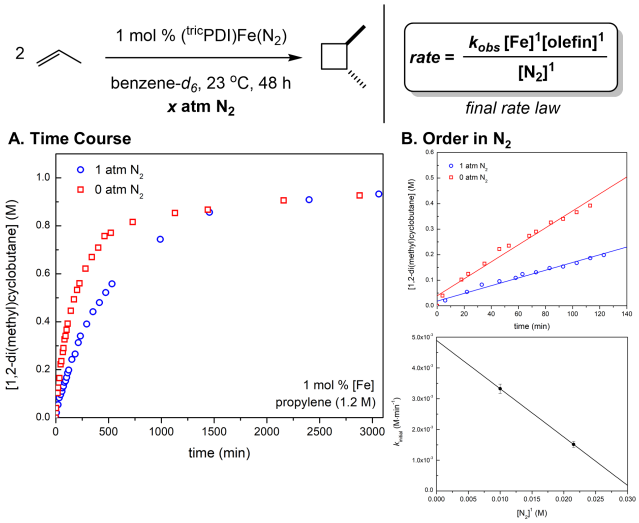

Figure 3. Kinetic analysis of iron-catalyzed [2+2] cycloaddition of propylene at 0 and 1 atm N_2. A. Time course of the reaction from 0 to 48 hours at 0 and 1 atm N_2. B. Initial rates plots for determining the order in N_2. 1 mol % [Fe] = 0.012 M. [N_2 – 1 atm] = 0.026 M, [N_2 – 0 atm] = 0.012 M (ratio of 2.15:1, initial rate ratio found = 2.19:1).

Natural Abundance ^{13}C KIE Measurements. As there are several mechanistic possibilities consistent with the observed rate law, measurement of kinetic isotope effects may shed light on irreversible bond-forming or -breaking processes during the reaction. Using the method described by Singleton and previously applied by our group in the iron-catalyzed [4+4] cycloaddition of dienes,[11,12] the ^{13}C KIE for formation of *trans*-1,2-dihexylcyclobutane was measured (Figure 4). Values near unity were obtained at all positions within the 4-membered ring and alkyl chains, consistent with no heavy atom KIE and the absence of Fe–C or C–C bond-forming or -breaking events in the first irreversible step of the reaction.

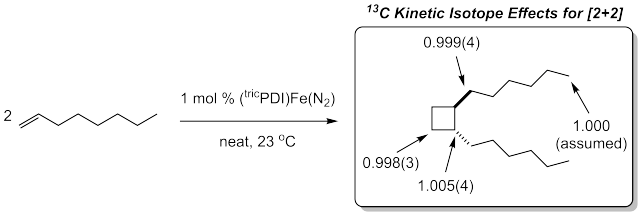

Figure 4. Results of natural abundance ^{13}C KIE analysis for iron-catalyzed [2+2] cycloaddition of 1-octene.

Observation of Catalyst Resting State and Degradation Species. To gain additional information about the catalytic cycle and iron speciation throughout the intermolecular [2+2] reaction, isolation of catalytically relevant organometallic intermediates was explored. Due to the high lipophilicity of ^{tric}PDI and the corresponding iron complexes, attempts to obtain single crystals suitable for X-ray diffraction studies have been unsuccessful. Analysis by ^{1}H NMR spectroscopy was similarly uninformative, as any spectra acquired under conditions similar to the catalytic cycloaddition reaction (i.e. **(^{tric}PDI)Fe(N_2)** in the presence of excess 1-octene or propylene) produced an array of signals that could not be deconvoluted. Freeze-quench ^{57}Fe Mössbauer spectroscopy was therefore used to determine the number and nature of iron compounds formed under catalytic conditions. In a typical procedure, the [2+2] cycloaddition of 1-octene was stirred for 10 minutes (approximately 5% conversion) and the sample rapidly frozen at 77

K and analyzed by ^{57}Fe Mössbauer spectroscopy (Figure 5). Because there is no induction period in the catalytic reaction, this early time point was chosen to avoid potential signal contamination from deactivation byproducts that form at higher conversion. A quadrupole doublet was observed with the parameters (δ = 0.37 mm/s; $|\Delta E_Q|$ = 0.66 mm/s)[13] being consistent with a (PDI)Fe(L)(N_2) compound where L can be N_2, PR_3, or an alkene.[14] These complexes are highly covalent and the electronic structure at iron is best be described as a hybrid between low-spin Fe(0) and Fe(II) coordinated to a closed-shell PDI ligand. The ambiguity of oxidation state is a result of the redox non-innocence of the PDI ligand and the high degree of π-back donation from iron.[9,15] These data, along with the rate law data, support **(^{tric}PDI)Fe(N_2)(η^2-1-octene)** as the catalyst resting state at early conversion to cyclobutane product.[16]

To corroborate both the electronic structure and spectroscopic data of **(^{tric}PDI)Fe(N_2)(η^2-1-octene)**, full molecule DFT calculations were performed. At the B3LYP level of theory, the lowest energy electronic configuration converged to a closed-shell, S = 0 solution, reflecting the structure of the proposed resting state. The DFT calculated ^{57}Fe Mössbauer parameters of δ = 0.45 mm/s and ΔE_Q = 0.81 mm/s are in good agreement with the experimental findings and within the generally accepted error range.[17]

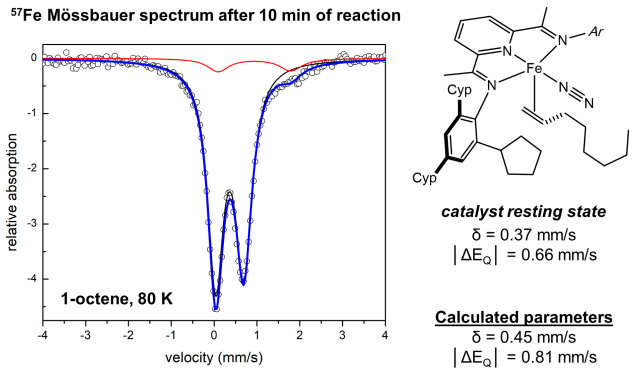

Figure 5. Freeze-quench zero-field ^{57}Fe Mössbauer spectrum of iron-catalyzed [2+2] reaction after 10 minutes of reaction.

To understand the origin of catalyst deactivation, similar analytical experiments were conducted to identify the iron products. Following the [2+2] cycloaddition reaction, the ligand was removed from iron by addition of water and the resulting isolated solid analyzed by ^{1}H NMR spectroscopy. As illustrated in Scheme 3, one of the cyclopentyl aryl substituents was converted to a cyclopentenyl group, establishing dehydrogenation of the ligand to **(dehydro-^{tric}PDI)**. A 1:1 mixture of olefin regioisomers (1-cyclopentenyl:2-cyclopentenyl) along with a stoichiometric amount of octane (with respect to the iron precatalyst) was also observed at the end of the reaction (the latter confirmed by gas chromatographic analysis of the reaction mixture), accounting for the loss of one equivalent of H_2 from the ligand. This indicates that **(^{tric}PDI)Fe(N_2)**, in analogy to other (PDI)Fe(N_2) complexes, ultimately undergoes transfer hydrogenation from ligand to α-olefin, although the rate of dehydrogenation is substantially slower for **(^{tric}PDI)Fe(N_2)**, which is in line with the observed [2+2] reactivity and slower catalyst degradation.[4d,18]

Scheme 3. Isolation of dehydrogenated PDI ligand.

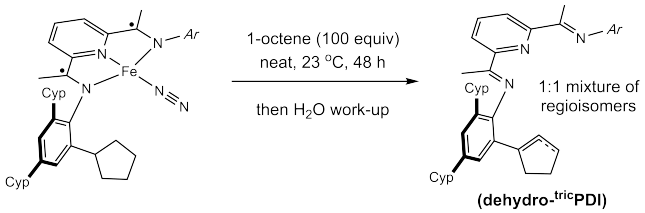

To investigate the mechanism of ligand dehydrogenation and to understand the coordination of **(dehydro-^{tric}PDI)** to iron during the catalytic reaction, freeze-quench ^{57}Fe Mössbauer experiments were performed. The iron-catalyzed [2+2] reaction was conducted for 8 hours and rapidly frozen at 77 K and then analyzed by ^{57}Fe Mössbauer spectroscopy (Figure 6). Two overlapping quadrupole doublets were observed in a 61:39 ratio with parameters δ = 0.32 mm/s and $|\Delta E_Q|$ = 1.94 mm/s and δ = 0.33 mm/s and $|\Delta E_Q|$ = 0.92 mm/s, respectively. The latter signal has parameters strikingly similar to (PDI)Fe(L)(N_2) compounds and **(^{tric}PDI)Fe(N_2)(η^2-1-octene)**, suggesting that the doublet corresponds to **(dehydro-^{tric}PDI)Fe(N_2)**, which likely exists as a mixture of two olefin regioisomers.[19] The major quadrupole doublet has parameters that suggest an intermediate spin Fe(II) or Fe(III) compound with an asymmetric ligand field, likely (PDI)FeX_2.[20] While an olefin-derived iron metallacycle is a possibility, it is unlikely given that little productive catalysis occurred at this conversion. The DFT-computed (B3LYP level of theory) ^{57}Fe Mössbauer parameters (δ = 0.25 and ΔE_Q = 2.04 mm/s) for the putative cyclometallated iron hydride, **(cyclomet-^{tric}PDI)Fe-H** with a BS(3,1) electronic configuration reproduce the experimental data. This compound, which likely exists as a mixture of isomers, is possibly an intermediate *en route* to dehydrogenation of the cyclopentyl ring.

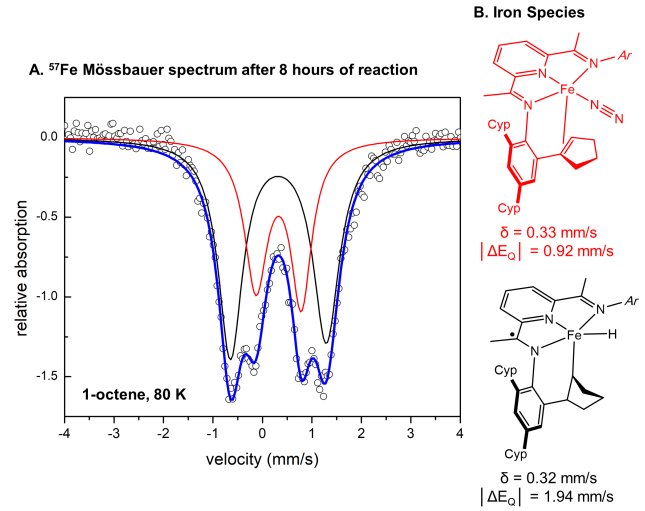

Figure 6. A. Freeze-quench zero-field ^{57}Fe Mössbauer spectrum of iron-catalyzed [2+2] reaction after 8 hours. B. Iron species in the spectrum (likely a mixture of regioisomers).

To confirm the identity of both the catalyst resting state and its degradation products, the [2+2] cycloaddition of 1-octene was also monitored by infrared spectroscopy as the N-N stretching region is diagnostic. As presented in Figure 7, aliquots of the iron-catalyzed [2+2] reaction were taken at 10 minutes, 4 hours, and 18 hours, and the solution samples analyzed by IR spectroscopy. At the 10 minute interval, a single band at 2117 cm^{-1} was observed assigned to **(^{tric}PDI)Fe(N_2)(η^2-1-octene)**. At 4 hours, two new stretches at 2096 and 2085 cm^{-1} were observed, likely arising from the two

regioisomers of **(dehydro-^{tric}PDI)Fe(N$_2$)**. Finally, after 18 hours of reaction, the stretch at 2117 cm^{-1} was absent but the bands at 2096 and 2085 cm^{-1} persisted supporting **(^{tric}PDI)Fe(N$_2$)(η^2-1-octene)** as the catalyst resting state that over time converts to the deactivated product, **(dehydro-^{tric}PDI)Fe(N$_2$)** by dehydrogenation of a cyclopentyl substituent.

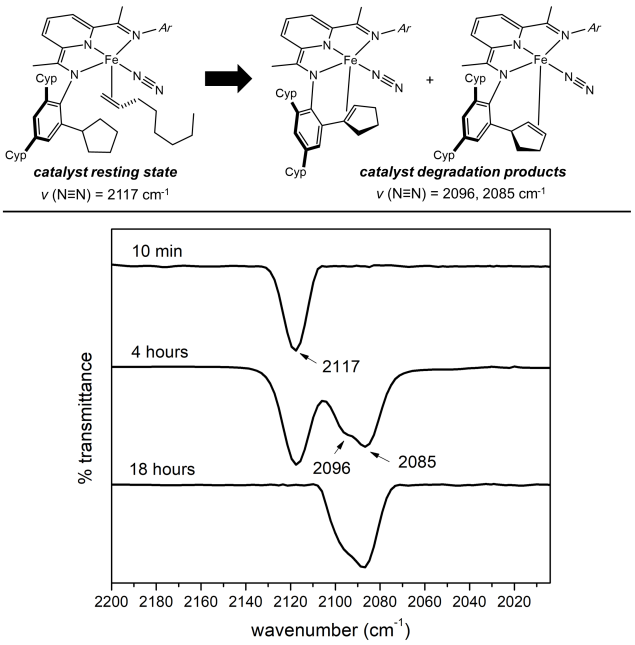

Figure 7. Top, progression of PDI iron speciation over the course of the iron-catalyzed [2+2] reaction. Bottom, solution infrared spectrum (1-octene, 23 °C) throughout the reaction (N_2 region).

As presented above, catalyst degradation, not inherently slow reactivity or unfavorable thermodynamics, was the cause for the lower yields of certain substrates in the iron-catalyzed alkene cyclodimerization. Support for this hypothesis was obtained from catalyst loading studies (Table 1). With 3 mol % **(^{tric}PDI)Fe(N$_2$)**, α-olefins including propylene, 1-hexene, and 1-octene underwent [2+2] cycloaddition in >98% yield and >99% regio- and diastereoselectivity after 24 hours. 4-Methyl-1-pentene, allylbenzene and homoallylbenzene similarly produced the corresponding *trans*-cyclobutanes in high yields (92%, 97%, and >98%, respectively) with >99% regio- and diastereoselectivity after 24 hours. As the reaction is first order in iron precatalyst, the increased catalyst loading likely increases the rate of reaction to surpass the rate of catalyst degradation by ligand dehydrogenation and allow for complete conversion of the olefins to the corresponding substituted cyclobutane.

Table 1. Iron-catalyzed [2+2] cycloaddition of alpha-olefins at two different catalyst loadings. *Indicates values taken from reference 4c.

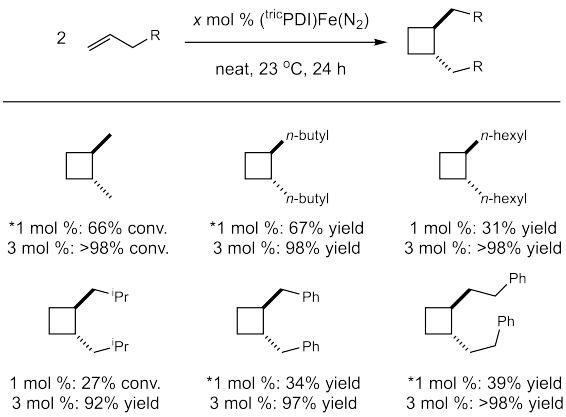

Proposed Catalytic Cycle. Based on a combination of the data disclosed in the previous section, a catalytic cycle for iron-catalyzed intermolecular [2+2] cycloaddition of α-olefins is proposed (Scheme 4). The lack of any detectable natural abundance ^{13}C KIE at any cyclobutane carbon of the product indicates that neither oxidative cyclization nor reductive elimination are the first irreversible steps, and therefore, potentially not rate-limiting. This suggests that ligand substitution, dissociation, or association are viable candidates for the rate-determining step. The freeze-quench ^{57}Fe Mössbauer and IR monitoring studies support **(^{tric}PDI)Fe(N$_2$)(η^2-1-octene)** as the catalyst resting state, consistent with rapid coordination of the first alkene to the precatalyst. Using the rapid pre-equilibrium approximation (assuming that $K_2 > k_3$) a rate law derived from the reaction mechanism presented in Scheme 4 matches that obtained from the kinetic data (rate = k_{obs}[Fe]^1[1-octene]^1[N$_2$]$^{-1}$).

Scheme 4. Proposed catalytic cycle for the iron-catalyzed intermolecular [2+2] cycloaddition of α-olefins. Rds = rate-determining step. *Ar* = 2,4,6-tricyclopentylaryl. R = hexyl. k_5 and $k_{5'}$ are possible turnover pathways of the cycle.

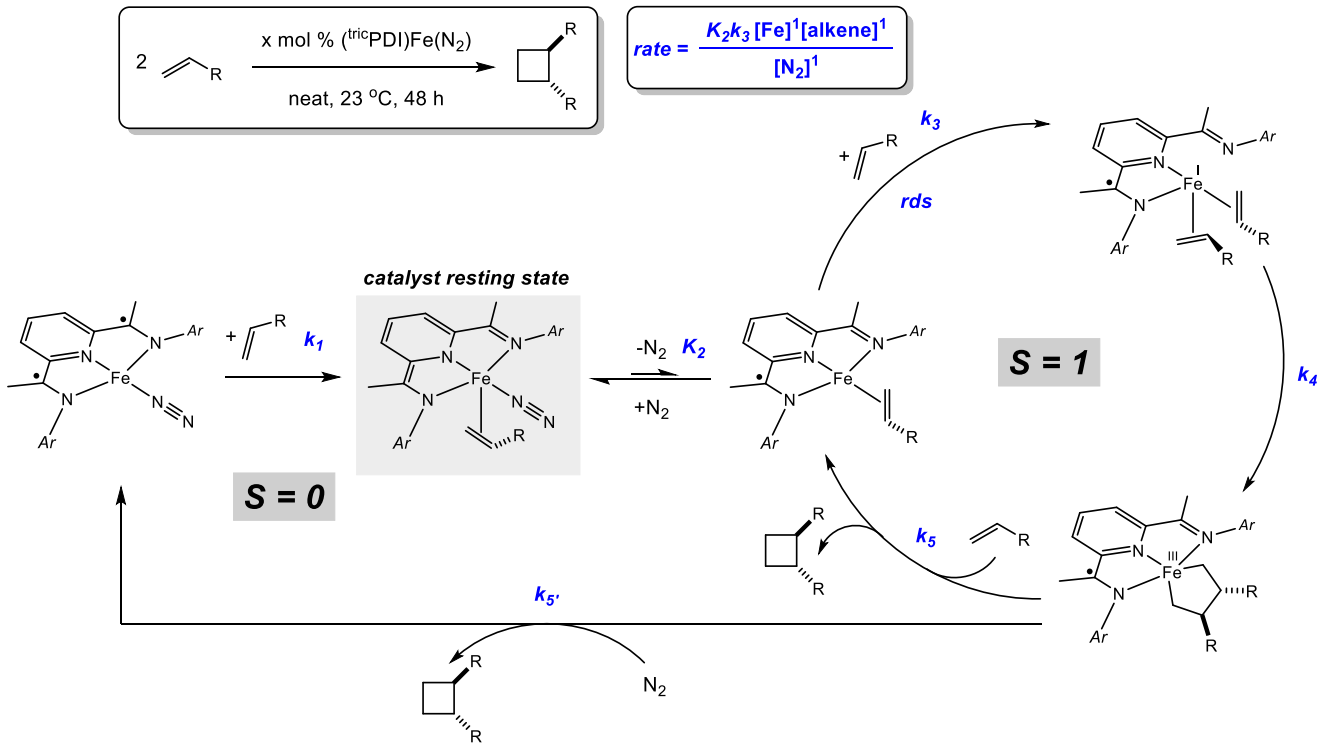

The reaction commences with formation of the catalyst resting state **(tricPDI)Fe(N₂)(η²-1-octene)** followed by unimolecular dissociation of N_2 from this complex to form **(tricPDI)Fe(η²-1-octene)**. This equilibrium process likely involves a spin-transition from $S = 0$ to $S = 1$ and precedes rate-determining association of 1-octene to the four-coordinate complex to form **(tricPDI)Fe(η²-1-octene)₂** where the PDI ligand has dissociated an imine arm and is bound κ².[21] This accounts for both the inverse order in N_2 concentration and the first-order dependence in 1-octene. The subsequent steps along the catalytic cycle are fast and likely include: oxidative cyclization to produce the ferrocyclopentane and reductive elimination of the resulting metallacycle to yield the cyclobutane product. Due to the high coordination affinity of N_2 to (tricPDI)Fe, it is difficult to know precisely how the catalyst turns over. Following reductive elimination, the coordinatively unsaturated iron catalyst can either coordinate 1-octene (Scheme 4, pathway with rate constant k_5), or uptake N_2 (Scheme 4, pathway with rate constants $k_{5'}$ and k_1).[9] While both routes are possible from a thermodynamic standpoint (see Figure S36 in the Supporting Information for details), it is ambiguous whether the catalyst resting state is on- or off-cycle, although N_2 pressure likely affects which turnover pathway is preferred (i.e. k_5 for low N_2 pressure and $k_{5'}$ for high N_2 pressure).

To better understand the persistence of **(tricPDI)Fe(N₂)(η²-1-octene)** and why direct olefin association to it is not observed, a more thorough analysis of the electronic structure of the catalyst resting state was performed. The DFT-calculated structure of **(tricPDI)Fe(N₂)(η²-1-octene)** supports a low-spin iron center bound to a doubly-reduced, redox non-innocent PDI ligand. The oxidation state ambiguity at iron is due to the strong π-back donation from iron to PDI.[9] Indeed, the highest occupied molecular orbital (HOMO) of the complex is an ad-mixture of a dz^2-type orbital localized on iron and a PDI π* orbital of B_2 symmetry (Figure 8). Normally dz^2 is a totally symmetric orbital and would therefore be unable to mix with an antisymmetric PDI orbital. However, the presented dz^2 orbital is the corresponding antibonding interaction of the parent Fe dz^2 orbital and the alkene π-orbital. This deforms the presented dz^2 orbital towards B_2 symmetry (causing the lobe opposite the alkene to enlarge, while the lobe pointed towards the alkene is diminished) and allows for mixing. The overall low symmetry of the molecule also aids in this mixing. The lowest occupied molecular orbital (LUMO) is the corresponding antibonding interaction between dz^2 and PDI π*, of which dz^2 only constitutes 17% of the total molecular orbital. Because the low energy, empty orbital required for ligand association at **(tricPDI)Fe(N₂)(η²-1-octene)** is largely ligand-based (instead of metal-based), combined with the fact that it is an 18-electron complex, the catalyst resting state likely cannot undergo associative ligand substitution. The most likely productive process is dissociation of N_2, consistent with the observed rate law.

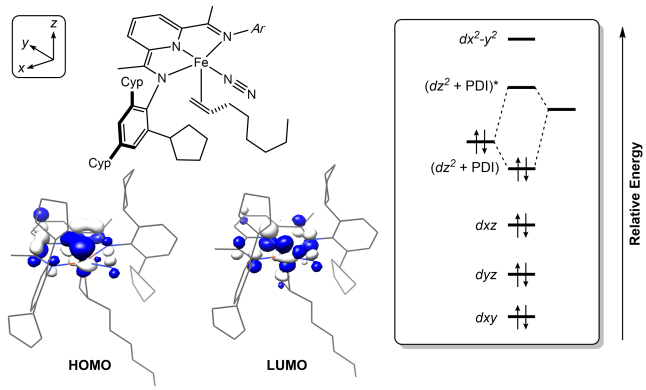

Figure 8. Qualitative frontier molecular orbital diagram of **(tricPDI)Fe(N₂)(η²-1-octene)** along with representations of the HOMO and LUMO of the complex.

While additional details of N_2 dissociation from **(tricPDI)Fe(N₂)(η²-1-octene)** are difficult to ascertain (as it

can involve a number of different steps, including imine dissociation before, after, or during spin transition), the net result of any pathway is formation of **(^{tric}PDI)Fe(η^2-1-octene)**. DFT calculations on **(^{dic}PDI)Fe(η^2-propylene)** were performed with B3LYP level of theory to better understand this four-coordinate complex (the octyl group was truncated to a methyl group and the tricyclopentylaryl groups were truncated to dicyclopentylaryl groups). The complex converged to a broken symmetry (1,1) solution where an $S = ½$ Fe(I) center is ferromagnetically coupled to an unpaired spin on the singly-reduced PDI ligand. The magnetic orbitals of **(^{dic}PDI)Fe(η^2-propylene)** are dz^2 and (dxz+PDI)*, which have a spatial overlap of $S = 0.04$, a remarkably low value due to the mismatched symmetry of the two orbitals, preventing effective overlap and coupling.[22] The relative energies of the singlet and triplet states of this complex differ by only by 2.1 kcal·mol^{-1}, favoring the triplet configuration. Due to this narrow singlet-triplet gap, it is difficult to accurately determine which spin state is lowest in energy[23] and whether spin-crossover occurs explicitly before or after N_2 dissociation, the latter scenario occurring via facile thermal access of the triplet state, not necessarily via spin-orbit coupling (see Supporting Information for preliminary computational studies on this process).

Upon formation of **(^{tric}PDI)Fe(η^2-1-octene)**, the 4-coordinate complex can either react productively with an alkene or unproductively with dinitrogen (and re-form the catalyst resting state). As mentioned above, N_2 likely has a higher binding constant for (^{tric}PDI)Fe than an alkene, corroborated by the observed inverse order in [N_2] for the [2+2] cycloaddition reaction. This results in association of 1-octene to **(^{tric}PDI)Fe(η^2-1-octene)** becoming the rate-determining step of the reaction. Additionally, the only molecular orbital of appropriate symmetry and energy for ligand association in **(^{tric}PDI)Fe(η^2-1-octene)** is dz^2, however this orbital is partially filled, which likely increases the kinetic barrier for 1-octene addition and further contributes to the step being rate-limiting.

Because C–C and Fe–C bond formation occur after the rate-determining step, it is difficult to experimentally determine the mechanism and molecularity of reductive elimination and oxidative cyclization in the intermolecular cycloaddition. It does, however, explain why intermolecular alkene-alkene cycloadditions are less efficient and more plagued by competing catalyst decomposition than those with conjugated and α,ω-dienes. Formation of the bis-olefin iron complex (which leads to the initial C–C bond formation) becomes the highest barrier of the reaction, manifesting itself in rate-determining addition of 1-octene to **(^{tric}PDI)Fe(η^2-1-octene)**. This brings the rate-constants of other pathways such as N_2 association and ligand C-H activation closer to that of C–C bond formation and leads to the observed rapid ligand dehydrogenation and inverse order in N_2. Improvements to alkene-alkene iron cycloaddition methodologies will include development of N_2-free reduced iron precatalysts, as well as increasing the binding affinity of alkenes over other ligands.

■ RESULTS AND DISCUSSION (INTRAMOLECULAR)

Representative Intramolecular Reaction. Investigations into the iron-catalyzed intramolecular [2+2] cycloadditions of alkenes were conducted with 1,7-octadiene as a representative substrate. As with the selection of 1-octene for the intermolecular variant, a boiling point of 117 °C makes the synthesis and isolation of deuterated isotopologues and isotopomers of the α,ω-diene more convenient and synthetically feasible (*vide infra*). In addition, 1,7-octadiene contains no heteroatoms to potentially complicate the coordination chemistry around iron. In the presence of 5 mol% **(^{tric}PDI)Fe(N_2)** in benzene-d_6, 1,7-octadiene underwent [2+2] cycloaddition to form *cis*-bicyclo[4.2.0]octane in >98% conversion and 92:8 d.r. after 9 hours at 23 °C (Figure 9, top). The major *cis* diastereomer is opposite the *trans* configuration observed from the intermolecular reaction. Thermodynamic parameters for the reaction, $\Delta G°$ = -8.9 kcal·mol^{-1}, $\Delta H°$ = -14.4 kcal·mol^{-1} and $\Delta S°$ = -14.7 cal·mol^{-1}·K^{-1} were computed by DFT (B3LYP level of theory) (Figure 9, top), where the entropic penalty of the unimolecular cycloaddition is significantly lower than the intermolecular variant. Furthermore, upon completion of the reaction, addition of more α,ω-diene re-initiated catalysis, demonstrating that deactivation of the iron compound is less pronounced with 1,7-octadiene as compared to 1-octene.

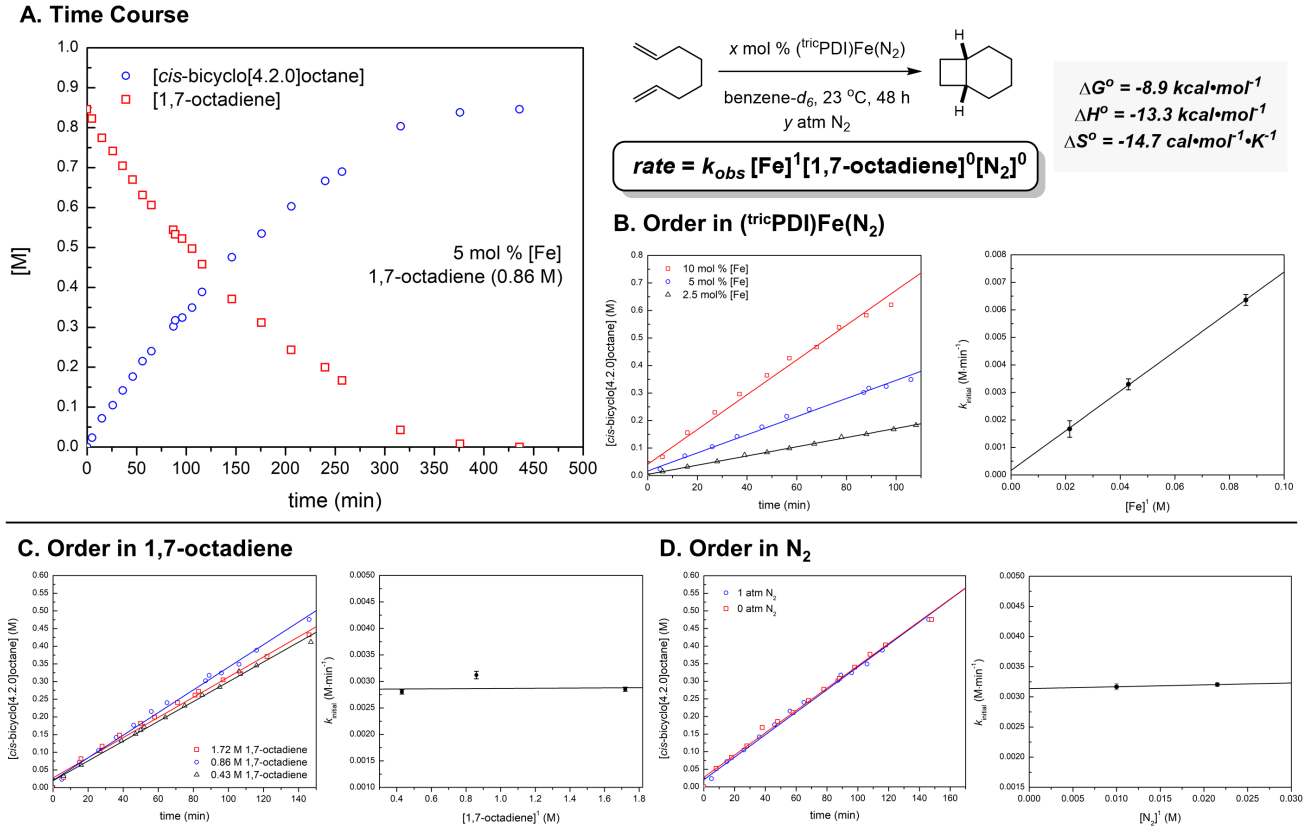

Figure 9. Kinetic analysis of iron-catalyzed intramolecular [2+2] cycloaddition of 1,7-octadiene. A. Time course of the reaction from 0 to 9 hours at 23 °C. B. Initial rates plots for determining the order in iron catalyst. C. Initial rates plots for determining the order in 1,7-octadiene. D. Initial rates plots for determining the order in N_2. y = 0 or 1 atm of N_2.

Kinetic Analysis. The rate law for the iron-catalyzed [2+2] cycloaddition of 1,7-octadiene was determined to gain mechanistic insight and for comparison to the intermolecular case. The catalytic reaction was monitored by ^{1}H NMR spectroscopy over the course of 9 hours at 23 °C ([**(tricPDI)Fe(N$_2$)**] = 0.043 M, [1,7-octadiene] = 0.86 M) and the time course presented in Figure 9A. The data support a well-behaved kinetic profile throughout the reaction with no evidence for an induction period or catalyst deactivation. The rate of the reaction is essentially constant throughout and only drops off towards the end of the reaction (low substrate concentration), suggesting saturation behavior with the α,ω-diene. The method of initial rates was used to determine the order in iron precatalyst, diene and nitrogen pressure (Figures 9B-D). The catalytic reaction was found to be first order in iron precatalyst and zeroth order in 1,7-octadiene and N_2 pressure.[24] The observed zeroth order in diene supports saturation kinetics and a catalyst-substrate complex as the resting state.[25]

Isolation and Characterization of Catalytically Relevant Iron Metallacycles. Because catalyst deactivation was minimal, the isolation of catalytically relevant intermediates was pursued. Attempts to obtain X-ray quality crystals from mixtures of **(^{tric}PDI)Fe(N$_2$)** and 1,7-octadiene were unsuccessful as the resulting iron complex(es) were too soluble in common organic solvents. To reduce lipophilicity and improve crystallinity, the ^{dic}PDI ligand (^{dic}PDI = 2,6-(2,6-dicyclopentyl)C$_6$H$_3$N=CMe)$_2$C$_5$H$_3$N)[26] was used instead. The resulting iron dinitrogen complex, **(^{dic}PDI)Fe(N$_2$)$_2$**, was catalytically competent for the [2+2] cycloaddition of 1,7-octadiene and produced the bicycle in similar yield and diastereoselectivity. Stirring a hexanes solution of **(^{dic}PDI)Fe(N$_2$)$_2$** with excess 1,7-octadiene produced a red solid that, after washing with pentane, afforded **(^{dic}PDI)Fe(bimetallacyclo[4.3.0]nonane)** in 41% yield (Scheme 5). The complex was characterized by a combination of solution-state magnetic measurements, X-ray diffraction, and ^{1}H NMR spectroscopy.

Scheme 5. Synthesis of (^{dic}PDI)Fe(*trans*-bimetallacyclo[4.3.0]nonane).

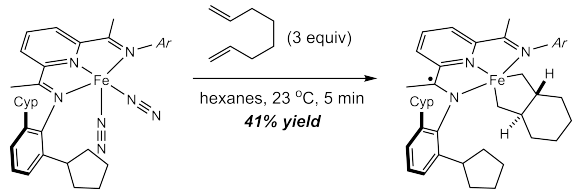

Single crystals suitable for X-ray diffraction studies were obtained from a concentrated pentane solution at -35 °C over 24 hours. A representation of the solid-state structure is presented in Figure 10, where the geometry at iron is best described as a distorted square-based pyramid (τ_5 = 0.35) with the three nitrogen atoms of the PDI ligand and the carbon *trans* to the pyridine comprising the basal plane of the complex. The C_{imine}–N_{imine} and C_{ipso}–C_{imine} bond distances are established metrics for determining the redox state of the pyridine(dimine) ligand.[27] For **(^{dic}PDI)Fe(*trans*-bimetallacyclo[4.3.0]nonane)**, C_{imine}–N_{imine} distances of 1.331(2) and 1.329(2) Å and C_{ipso}–C_{imine} values of 1.427(2) and 1.430(2) Å are consistent with a singly-reduced form of the chelate, supporting an Fe(III) oxidation state. The data were of sufficient

quality that the hydrogen atoms of the bimetallacycle were located freely and refined, allowing for unambiguous assignment of the stereochemistry of the bimetallacycle. Notably, the hydrogens are in a *trans* configuration, the opposite orientation of the diastereomer obtained from the catalytic reaction. Grubbs and co-workers reported nickel bimetallacyclo[4.3.0]nonane complexes that interconverted between the *cis* and *trans* isomers of the bimetallacyle at 0 °C,[28] suggesting that isomerization of metallacyclic intermediates in the current iron-catalyzed intramolecular [2+2] cycloaddition reaction may also be operative (*vide infra*). To reduce strain and accommodate the *trans* stereochemical arrangement, the cyclohexane ring of the bicycle adopts a chair conformation, while the metallacyclopentane ring adopts a half-chair conformation.

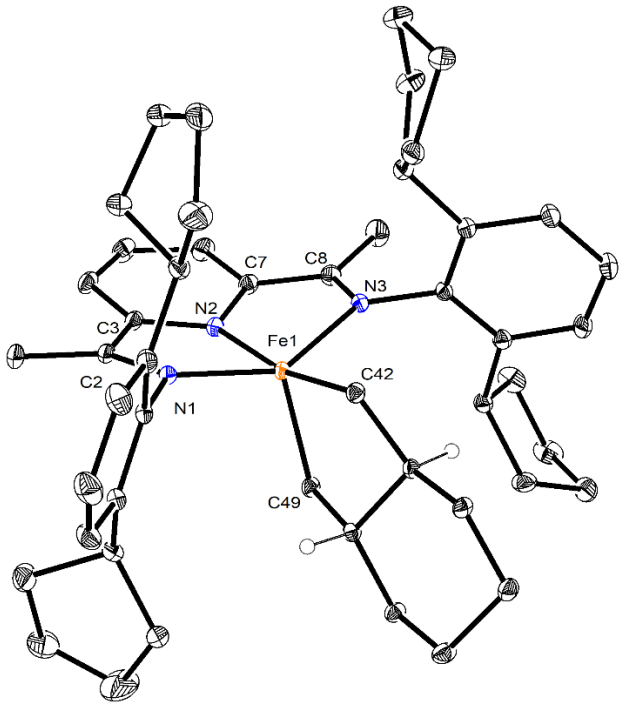

Figure 10. Representation of the solid-state structure of **(^{dic}PDI)Fe(*trans*-bimetallacyclo[4.3.0]nonane)** with thermal ellipsoids at 30% probability. Hydrogen atoms (except for those at the ring juncture of the bimetallacycle) omitted for clarity. Selected bond distances (Å) and angles (deg): Fe1 – N1 2.040(1), Fe1 – N2 1.908(1), Fe1 – N3 2.038(1), N1 – C2 1.331(2), N3 – C5 1.329(2), C2 – C3 1.427(2), C4 – C5 1.430(2), Fe1 – C10 2.024(1), Fe1 – C17 2.047(1); N1 – Fe1 – N2 78.09(4), N1 – Fe1 – N3 145.65(4), N2 – Fe1 – N3 77.73(4), N2 – Fe1 – C10 166.51(5), N1 – Fe1 – C10 99.17(5), N3 – Fe1 – C10 98.69(5), N2 – Fe1 – C17 108.78(5), C10 – Fe1 – C17 84.69(5).

Attempts to obtain a ^{1}H NMR spectrum of **(^{dic}PDI)Fe(*trans*-bimetallacyclo[4.3.0]nonane)** in benzene-d_6 were unsuccessful, as the complex underwent rapid reductive elimination to form *cis*-bicyclo[4.2.0]octane in 93:7 d.r. along with **(^{dic}PDI)Fe(N_2)$_2$** (Scheme 6). These observations support conversion of the observed *trans*-metallocycle to the more reactive *cis* isomer which has a lower barrier for C(sp^3)–C(sp^3) reductive elimination. In the presence of a slight excess of 1,7-octadiene, a single paramagnetic species with a signal range from -20 to 120 ppm was observed along with the α,ω-diene and product. The most isotropically shifted signals correspond to protons located on the pyridine and imine methyl groups of the pyridine(diimine) chelate and the methylene protons alpha to iron, due to enhanced spin polarization at these positions.[29] The observed number of peaks is consistent with a C_s symmetric molecule, suggesting the bimetallacycle undergoes rapid ring flips on the NMR time scale. A solution-state magnetic moment of 2.9(1) μ_B was measured at 23 °C (Evans' method, benzene-d_6), consistent with two unpaired electrons and an S = 1 ground state. The magnetic data, in combination with metrical data from X-ray diffraction studies support **(^{dic}PDI)Fe(*trans*-bimetallacyclo[4.3.0]nonane)** as an intermediate spin Fe(III) (S_{Fe} = 3/2) compound ligated to a singly reduced pyridine(diimine) chelate, leading to the observed S = 1 ground state. Although isolation of **(^{tric}PDI)Fe(*trans*-bimetallacyclo[4.3.0]nonane)** was difficult, the ^{1}H NMR spectrum and solution magnetic moment measurements are similar to those of the (^{dic}PDI) variant.

Scheme 6. Rapid reductive elimination of *cis*-bicyclo[4.2.0]octane from (^{dic}PDI)Fe(*trans*-bimetallacyclo[4.3.0]nonane) in solution at 23 °C.

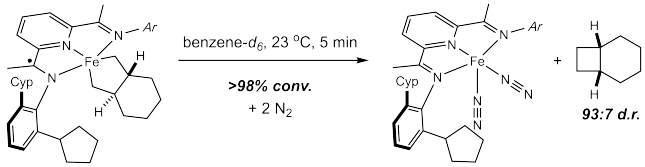

To gain insight into the electronic structure of **(^{dic}PDI)Fe(*trans*-bimetallacyclo[4.3.0]nonane)**, full-molecule DFT studies were conducted using the B3LYP level of theory. The complex converged to a broken symmetry (3,1) solution where the resulting Mulliken spin density plot was also generated and supports an intermediate-spin Fe(III) center antiferromagnetically coupled to a spin delocalized over the pyridine(diimine) chelate with minor contributions from the Fe–C orbitals of the metallacycle (Figure 11). Because *d*-orbitals make such a significant contribution to the two magnetically coupled orbitals of the molecule, there is both positive and negative spin density at iron. Examination of the qualitative *d*-orbital splitting diagram identified the magnetically coupled orbitals as both having d_{yz} parentage, with the spin up orbital containing significant contributions from a PDI π* orbital (due to strong π-back donation) and the spin down orbital containing significant contributions from a d_{yz} orbital mixed with Fe – C σ bonding orbitals of the metallacycle (Figure 12).

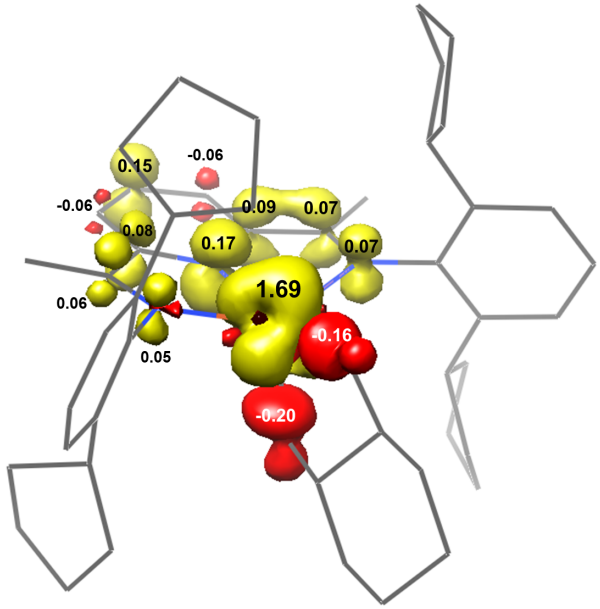

Figure 11. Mulliken spin density plot of (^{dic}PDI)Fe(*trans*-bimetallacyclo[4.3.0]nonane)

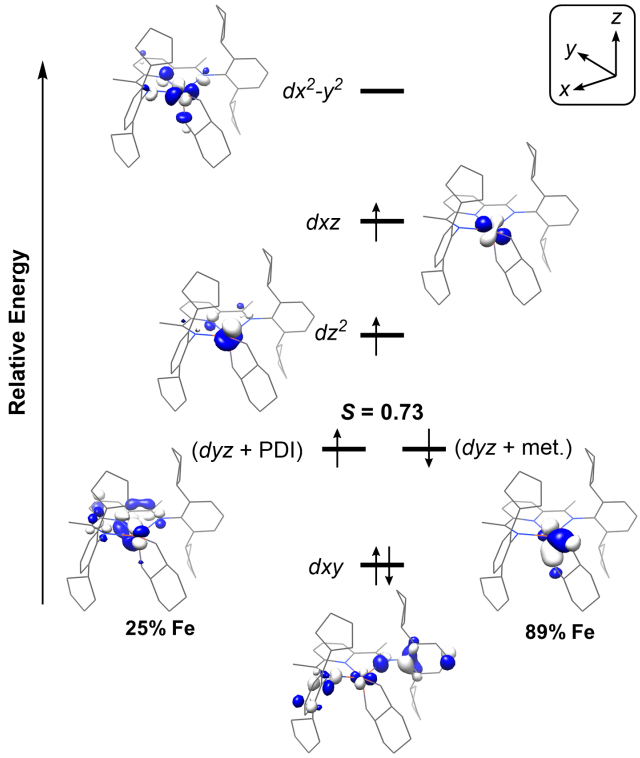

Figure 12. Qualitative *d*-orbital splitting diagram for (^{dic}PDI)Fe(*trans*-bimetallacyclo[4.3.0]nonane).

Due to the propensity of (^{dic}PDI)Fe(*trans*-bimetallacyclo[4.3.0]nonane) to undergo reductive elimination and the scarcity of (^{dic}PDI), sufficient quantities of the compound for a zero-field ^{57}Fe Mössbauer spectrum were not available. DFT-generated ^{57}Fe Mössbauer parameters of δ = 0.34 mm/s and ΔE_Q = 2.14 mm/s are in agreement with PDI iron metallacycles.[5] To ensure accuracy of these DFT calculations and to investigate whether other PDI ligands support *trans*-bimetallacyclo[4.3.0]nonanes (or whether ^{dic}PDI is unique in this regard), the synthesis of the corresponding metallacycle with $^{iPr(TB)}$PDI ($^{iPr(TB)}$PDI = 2,6-(2,6-(diisopropyl)C_6H_3N=C$(CH_2)_3)_2(C_5HN)$) was explored. Previous work has demonstrated that bis-olefin and metallacycle iron complexes of this chelate are more crystalline and less reactive than untethered variants.[5] Using conditions similar to those used for the synthesis of the ^{dic}PDI variant, ($^{iPr(TB)}$PDI)Fe(*trans*-bimetallacyclo[4.3.0]nonane) was isolated as a red solid in 72% yield (Scheme 7). The complex was stable in solution for extended periods of time (>48 hours) and the benzene-d_6 NMR spectrum was remarkably similar to (^{dic}PDI)Fe(*trans*-bimetallacyclo[4.3.0]nonane), containing 19 paramagnetically shifted signals from -20 to 150 ppm, supporting analogous solution-state structure for the ^{dic}PDI and $^{iPr(TB)}$PDI variants. A solution magnetic moment of 2.9(1) μ_B, was measured at 23 °C (Evans' method) supporting an S = 1 ground state.

Scheme 7. Synthesis of ($^{iPr(TB)}$PDI)Fe(*trans*-bimetallacyclo[4.3.0]nonane).

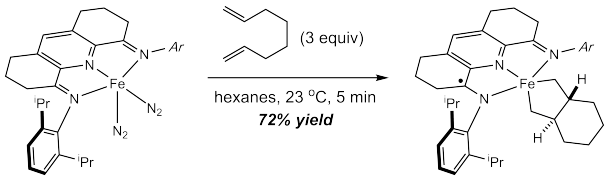

Single crystals suitable for X-ray diffraction studies were obtained from a concentrated pentane solution at -35 °C over 24 hours. The solid-state structure of ($^{iPr(TB)}$PDI)Fe(*trans*-bimetallacyclo[4.3.0]nonane) supports a distorted square-based pyramid geometry at iron (τ_5 = 0.38) and is analogous to the ^{dic}PDI variant (see Supporting Information for a representation of the solid-state structure). All these data support the assertion that, aside from its reduced reactivity, both ($^{iPr(TB)}$PDI) and (^{dic}PDI)Fe(bimetallacyclo[4.3.0]nonane) have identical solution-state, solid-state, and electronic structures. The zero-field ^{57}Fe Mössbauer spectrum of ($^{iPr(TB)}$PDI)Fe(bimetallacyclo[4.3.0]nonane) was recorded at 80 K in the solid state and is presented in Figure 13. An isomer shift of 0.31 mm/s and a quadrupole splitting of 2.83 mm/s were obtained, parameters that correlate well with the calculated values found for (^{dic}PDI)Fe(bimetallacyclo[4.3.0]nonane), as well as other pyridine(diimine) iron metallacycles previously reported.[5]

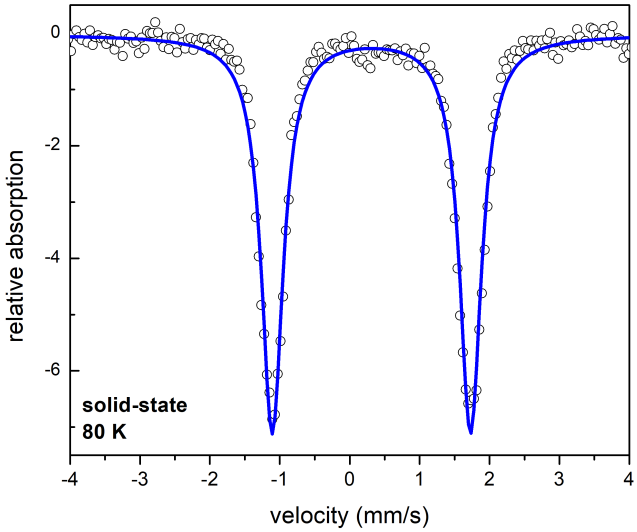

Figure 13. Solid-state zero-field ^{57}Fe Mössbauer spectrum of **($^{iPr(TB)}$PDI)Fe(*trans*-bimetallacyclo[4.3.0]nonane)**. Acquired at 80 K.

As stated previously, **($^{iPr(TB)}$PDI)Fe(*trans*-bimetallacyclo[4.3.0]nonane)** is stable in benzene-d_6 with no evidence for reductive elimination. It is likely that introduction of alkyl substitution at the 3 and 5 positions of the pyridine ring generates a more electron rich iron center, raising the barrier for C(sp^3)–C(sp^3) reductive elimination. To induce C–C bond formation, a benzene-d_6 solution of **($^{iPr(TB)}$PDI)Fe(bimetallacyclo[4.3.0]nonane)** was exposed to 1 atm of CO. An immediate color change to blue was observed with concomitant formation of *trans*-bicyclo[4.2.0]octane in >99:1 d.r. (Scheme 8). The higher selectivity of the stoichiometric C–C bond-forming reaction as compared to the catalytic variant (92:8 d.r.) suggests that CO-induced reductive elimination is more rapid than unimolecular reductive elimination of the bimetallcycle during the catalytic [2+2] cycloaddition reaction and prevents any isomerization of the bimetallacycle.

Scheme 8. Addition of CO to ($^{iPr(TB)}$PDI)Fe(*trans*-bimetallacyclo[4.3.0]nonane).

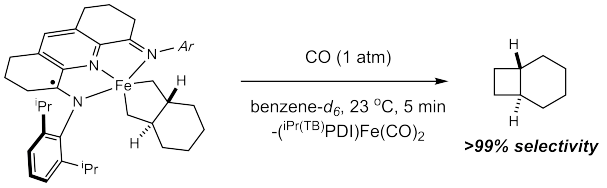

To gain additional information about the product- and selectivity-determining step of the intramolecular [2+2] reaction, the ^{13}C/^{12}C kinetic isotope effect was measured for the formation of natural abundance *cis*-bicyclo[4.2.0]octane. Because the resting state of the catalyst is the *trans*-bimetallacycle, there are two possibilities for the first irreversible step of the reaction (Scheme 9, left). The first is irreversible isomerization from *trans*- to *cis*-bimetallacycle followed by rapid reductive elimination, giving rise to a small KIE (either primary or inverse) at all carbons of the cyclobutane.[30] The second possibility is rapid equilibration of the *trans*- and *cis*-bimetallacycles followed by irreversible reductive elimination, where a primary KIE at the terminal cyclobutane carbons would be expected.[11b] Indeed, a primary ^{13}C kinetic isotope effect of 1.022(4) was measured at 23 °C for the terminal cyclobutane carbon of *cis*-bicyclo[4.2.0]octane, supporting unimolecular reductive elimination that is both irreversible and selectivity-determining (Scenario 2). No other significant KIE values were measured at any other carbon of the bicycle. Rapid and reversible equilibration of the *trans*- and *cis*-bimetallacyles before irreversible reductive elimination and possible Curtin-Hammett kinetics are also consistent with the observed diastereoselectivity of the reaction.

Scheme 9. Possible kinetic isotope scenarios for different irreversible steps in the iron-catalyzed [2+2] cycloaddition of 1,7-octadiene (left). Observed ^{13}C KIE values for *cis*-bicyclo[4.2.0]octane (right).

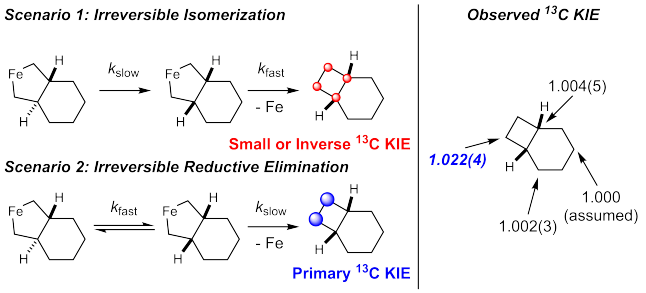

Proposed Catalytic Cycle. The combination of the kinetic data, identification of the catalyst resting state, and a primary ^{13}C kinetic isotope effect, support the catalytic cycle proposed in Scheme 10. As the rate law has no dependence on diene concentration nor N_2 pressure, this suggests that neither is involved in the isomerization of the bimetallacycle nor reductive elimination and that both processes are unimolecular. Any substitution reactions or equilibria that involve 1,7-octadiene or N_2 occur before formation of the catalyst resting state and are, therefore, kinetically irrelevant. Using the steady-state approximation and saturation kinetics (i.e. [Fe] = [catalyst resting state]), a rate law for the mechanism presented in Scheme 10 was derived and matches that obtained from the kinetic analyses. **(^{tric}PDI)Fe(N$_2$)** rapidly reacts with 1,7-octadiene to form **(^{tric}PDI)Fe(η^2:η^2-1,7-octadiene)**, which undergoes oxidative cyclization to produce **(^{tric}PDI)Fe(*trans*-bimetallacyclo[4.3.0]nonane)**, the catalyst resting state. An equilibrium between *trans*- and *cis*-diastereomers of the bimetallacycle precedes rate-limiting, unimolecular reductive elimination to furnish predominantly the *cis*-product (due to $k_6 >> k_5$). Rapid recombination of the iron catalyst and substrate regenerate the pyridine(diimine) bis-olefin complex and turn over the cycle.

Scheme 10. Proposed catalytic cycle for the iron-catalyzed intramolecular [2+2] of 1,7-octadiene. rds = rate-determining step. *Ar* = 2,4,6-tricyclopentylaryl.

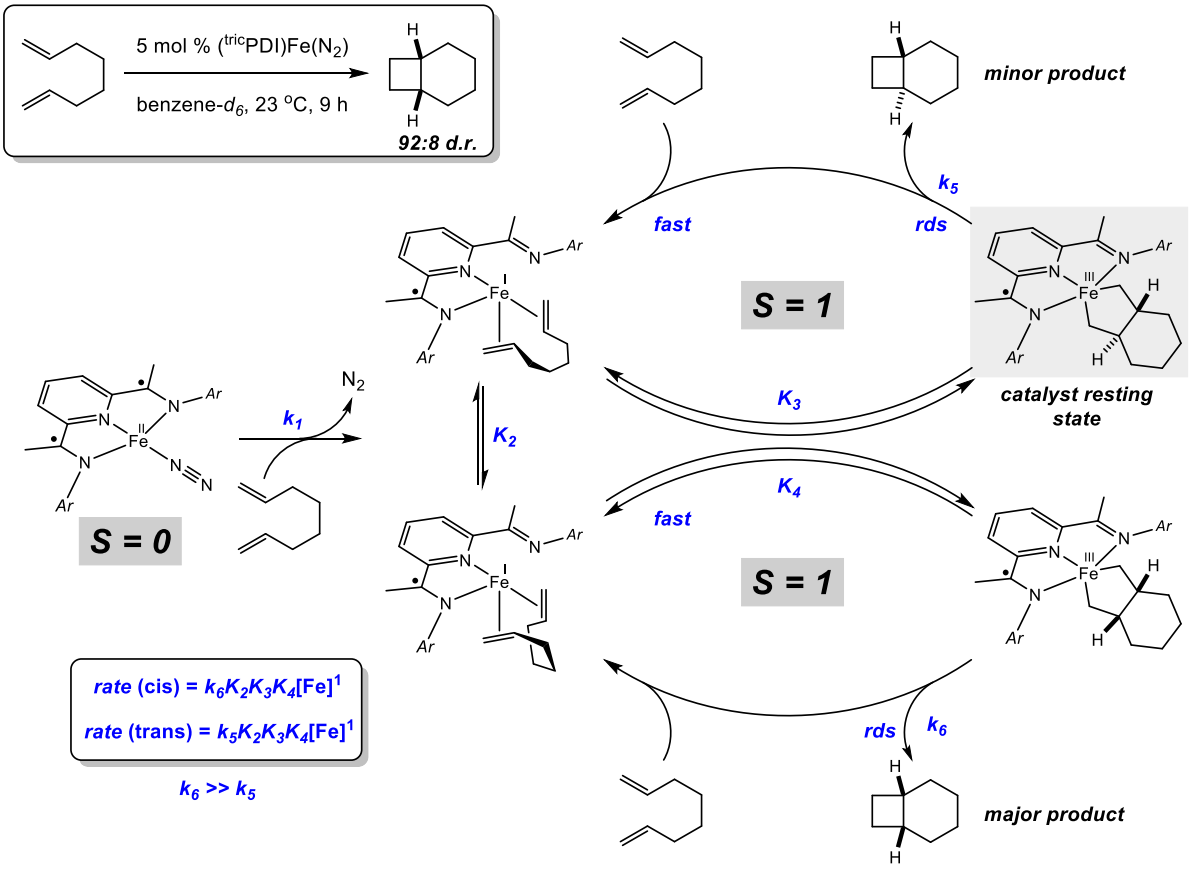

Due to the chelate effect, 1,7-octadiene has a stronger coordination affinity to [(tricPDI)Fe] than 1-octene, significantly lowering the barrier for N_2 displacement from **(tricPDI)Fe(N₂)** and alkene association to a putative **(tricPDI)Fe(η²-1,7-octadiene)**, making the corresponding rate constants to these processes kinetically inconsequential. This causes a shift in the catalyst resting state and the rate-determining step of the reaction. This phenomenon also explains the reduced catalyst decomposition rates observed in intramolecular [2+2] reactions: the iron catalyst is more likely to exists as a 1,7-octadiene adduct (either as the bis-olefin complex or the bimetallacycle), than interact with a cyclopentyl group on the ligand and undergo dehydrogenation.

Another question that arises in the proposed catalytic cycle is, why is the resting state of the intramolecular [2+2] cycloaddition the *trans*-bimetallacycle, while the product is predominantly the corresponding *cis*-bicycle? As the proposed catalytic cycle includes the equilibration of two diastereomeric bimetallacycles before the rate-determining step and a distribution of both products is formed (92:8 d.r.), a Curtin-Hammett scenario is likely to exist.[31] A reaction coordinate diagram describing this Curtin-Hammett scheme: interconversion of *trans*- and *cis*-bimetallacycles and their respective reductive elimination pathways to form their respective bicycles, is presented in Scheme 11 (the equilibration of *trans*- and *cis*-bimetallacycles is simplified to a single step). $\Delta\Delta G^{\ddagger}$ can be calculated from the diastereomeric ratio of bicyclo[4.2.0]octane formed during the reaction and is equal to 1.4 kcal·mol^{-1} favoring the *cis* diastereomer. Utilizing the Eyring equation and kinetic data obtained for the [2+2] cycloaddition of 1,7-octadiene, the total barrier for reductive elimination from the *trans*-metallacycle (the catalyst resting state) to the *cis*-product can be obtained and is equal to 23.1 kcal·mol^{-1} (at 23°C). This value does not correspond to $\Delta G^{\ddagger}_{cis}$, but the sum of $\Delta G^{\ddagger}_{cis}$ and the energy difference between the *trans*- and the *cis*-bimetallacycles (ΔG_{met}). Using DFT methods (B3LYP level of theory), ΔG_{met} was calculated to be 3.7 kcal·mol^{-1}, with the *trans*-diastereomer having the lower ground state energy, reflecting the observed isolation of only **(dicPDI)Fe(*trans*-bimetallacyclo[4.3.0]nonane)**. Qualitatively, the *cis*-bimetallacycle should be higher in energy than the *trans*-isomer as it contains two additional gauche butane interactions within the cyclohexane ring (each worth approximately 0.9 kcal·mol^{-1}),[32] in addition to the steric interaction with one of the 2,4,6-tricyclopentylaryl groups on the pyridine(diimine) ligand (none of which are present in the *trans*-isomer). Applying both the experimental and computational values, $\Delta G^{\ddagger}_{cis}$ = 19.4 kcal·mol^{-1} and $\Delta G^{\ddagger}_{trans}$ = 24.5 kcal·mol^{-1} were obtained and indicate that while the *trans*-bimetallacycle is lower in energy, the transition state for reductive elimination from the *cis*-bimetallacycle is lower in energy, explaining the observed preference for formation of *cis*-bicyclo[4.2.0]octane.[33] During the synthesis of **(dicPDI)Fe(*trans*-bimetallacyclo[4.3.0]nonane)**, the equilibrium between the *trans*- and *cis*-bimetallacycles is likely perturbed by the low solubility of the *trans*-isomer in hexanes, which precipitates the product, slows isomerization/reductive elimination, and allows for isolation.

Scheme 11. Curtin-Hammett scenario for the reductive elimination of bicyclo[4.2.0]octane from (^{dic}PDI)Fe(bimetallacyclo[4.3.0]nonane). "Fe" = (^{dic}PDI)Fe.

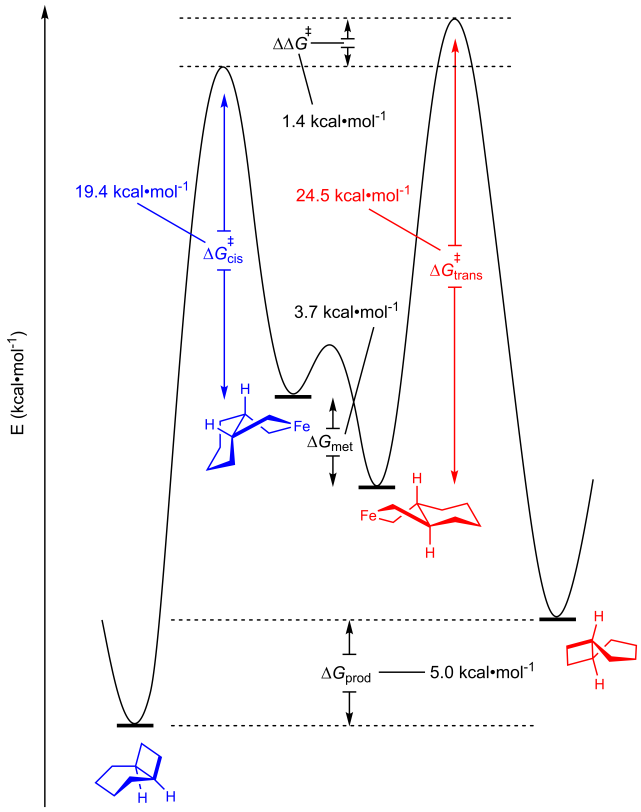

When comparing the inter- to the intramolecular iron-catalyzed [2+2] cycloadditions, the most obvious difference is the change in diastereoselectivity of the 1,2-cyclobutane: the intermolecular reaction is *trans*-selective while the intramolecular is *cis*-selective. As there is less experimental data on the product-forming step of the intermolecular [2+2] cycloaddition reaction, we currently do not know the precise origin of this change in selectivity. While the DFT-computed (B3LYP) ground-state energy difference between ***cis***- vs. ***trans***-**(^{dic}PDI)Fe(2,3-dimethylmetallacyclopentane)** is 6.7 kcal·mol^{-1} favoring the *trans*-isomer (an even more pronounced preference than in the intramolecular case), this is by no means definitive as it reveals nothing about the difference in transition state energies for reductive elimination of the two metallacycles. A high barrier for *trans*-to-*cis* metallacycle isomerization is a possible explanation for the observed exclusive *trans*-selectivity, while another is that the relative stereochemistry of the metallacycle (and therefore the product) is determined during the rate-determining step of the reaction: olefin coordination to **(^{tric}PDI)Fe(η^2-alkene)**. The *trans*-selectivity could then be explained via a straightforward steric argument, as the incoming alkene would coordinate to give a *trans* arrangement of the olefin R-groups to minimize interactions with each other and the imine aryl groups on the PDI ligand.

In the [2+2] cycloaddition of 1,7-octadiene, reductive elimination is likely unimolecular and therefore, not ligand-induced, as was reported for the PDI iron-catalyzed cross [2+2] cycloaddition of dienes and alkenes.[4d] Additionally, while we cannot know the precise molecularity of reductive elimination in the [2+2] cycloaddition of 1-octene, as this step occurs after rate-determining olefin association to **(^{tric}PDI)Fe(η^2-1-octene)**, we can surmise that it is analogous to the intramolecular case. Attempts to calculate a potential ligand-induced (N_2, alkene, α,ω-diene, etc.) reductive elimination pathway from PDI iron metallacycles or bimetallacycles was unsuccessful, as no global minima were located. In the next section, experiments are detailed to probe the mechanism of reductive elimination.

■ STUDIES ON REDUCTIVE ELIMINATION

Investigations into the Reductive Elimination Step of [2+2] Cycloadditions. To better understand the pathway for C(sp^3)–C(sp^3) reductive elimination in both inter- and intramolecular [2+2] cycloadditions, experiments were devised that would allow probes of a stepwise or concerted process. A "stepwise" mechanism is defined as initiating with Fe–C bond homolysis, generation of a carbon-centered radical followed by radical recombination to both cleave the second Fe–C bond and form the cyclobutane product.[34] As proposed in Scheme 12, generating metallacycles from stereodefined, deuterated olefins allows for the differentiation of both pathways. In a concerted pathway, any relative stereochemistry between the deuteria and other groups on the ring should be retained in the cyclobutane product and a single isotopomer should be observed. Conversely, if a stepwise mechanism is operative, generation of carbon-centered radicals would epimerize the stereocenters and a mixture of isotopomers would be observed. To perform these experiments, both 1-deutero-*E*-1-octene and 1,8-dideutero-*E,E*-1,7-octadiene were synthesized and subjected to catalytic cycloaddition conditions.

Scheme 12. A. Summary of inter- and intramolecular iron-catalyzed [2+2] cycloadditions examined in this article. B. Possible strategy for distinguishing between reductive elimination pathways.

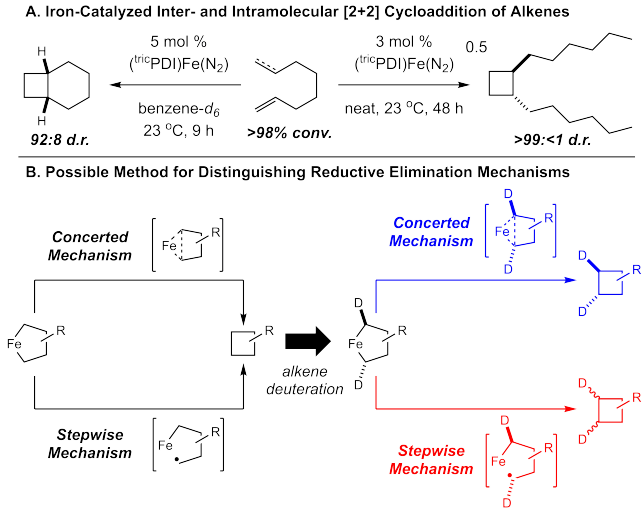

Deuterium Labelling Studies: 1-octene. Exposure of 1-deutero-*E*-1-octene to the intermolecular [2+2] cycloaddition conditions produced *trans*-1,2-dihexylcyclobutane in 23% yield and a combination of ^{1}H and ^{2}H NMR and mass spectrometry (GC-MS in EI mode) was used to determine the distribution of deuterium in the product as well as any isotopomers that formed in the reaction (results presented in Figure 14). The product was a complex mixture of isotopomers with deuterium incorporated statistically around all carbon positions of the cyclobutane ring, with no incorporation along the alkyl chain of the product. Mass spectrometry

established that the product was also a mixture of isotopologues, with only 29% of the material corresponding to the dideutero product (the expected isotopologue) and the rest being a mixture from d_0-d_5-1,2-dihexylcyclobutane. As stated previously in this article, ligand cyclometallation is a likely initiation pathway for catalyst degradation and could also be the source of deuterium scrambling. To confirm this hypothesis, **(dehydro-^{tric}PDI)** was also isolated from the reaction mixture and examined by a combination of ^{2}H NMR spectroscopy and high-resolution mass spectrometry (LC-MS, ESI mode). Indeed, the ligand was found to be a complex mixture of isotopologues ranging from d_0 to d_9. D-incorporation was also observed at multiple positions across both the cyclopentyl and cyclopentenyl groups of **(dehydro-^{tric}PDI)**.

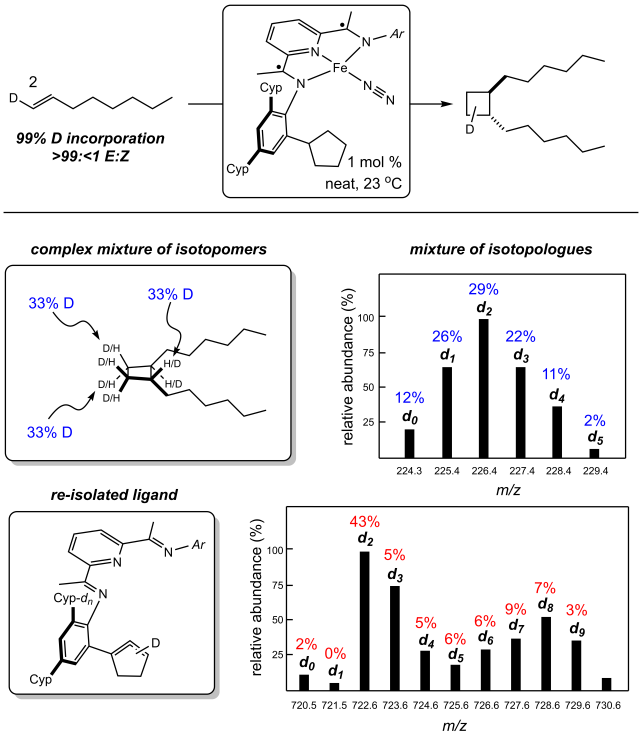

Figure 14. Iron-catalyzed [2+2] cycloaddition of 1-deutero-*E*-1-octene and techniques to determine number of isotopologues and isotopomers. The mass spectrum histograms are representations of the originals, which can be found in the Supporting Information.

To probe the relative rate of cyclometallation with **(^{tric}PDI)Fe(N$_2$)**, 20 equivalents of 1-deutero-*E*-1-octene were added to the iron precatalyst and the reaction monitored by ^{1}H NMR spectroscopy (Scheme 13). After 10 minutes at 23 °C, deuterium scrambling was observed at both the 1- and 2-positions of the olefin, leading to a statistical mixture after 2 hours.[xi] While difficult to distinguish by ^{1}H NMR spectroscopy, the presence of up to d_5-1,2-dihexylcyclobutane indicates that d_2- and d_3-1-octene are likely also formed. This NMR experiment and the previous deuterium labelling study indicated that cyclometallation occurred on the same time-scale as productive [2+2] cycloaddition, and that it is likely reversible, accounting for deuterium incorporation at multiple positions of both the PDI ligand and the alkene. This also demonstrates that tracking deuterium incorporation from starting material to product cannot be used to deconvolute the mechanism of C(sp^3)–C(sp^3) reductive elimination in intermolecular [2+2] cycloadditions, as it is immediately complicated by ever-present ligand-cyclometallation.

Scheme 13. Addition of 1-deutero-*E*-1-octene to (^{tric}PDI)Fe(N$_2$).

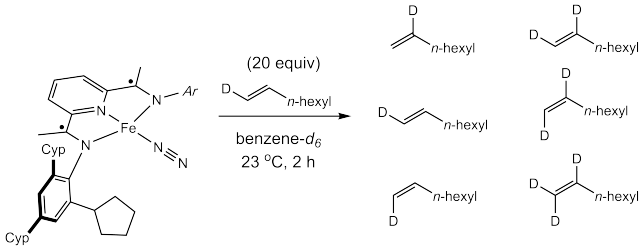

Deuterium Labelling Studies: α,ω-dienes. A similar deuterium labelling study was performed for the iron-catalyzed intramolecular [2+2] cycloaddition of 1,8-dideutero-*E,E*-1,7-octadiene. Under the standard reaction conditions, *cis*-bicyclo[4.2.0]octane was formed in 75% yield as a mixture of both isotopologues and isotopomers. Analysis by ^{2}H NMR spectroscopy revealed that deuterium was distributed statistically over all cyclobutane carbons, similar to the intermolecular case (Figure 15). Mass spectrometry (GC-MS, EI mode) also indicated that a mixture of isotopologues was also formed with only 37% of the total product corresponding to the dideutero product. (^{tric}PDI) isolated following the catalytic reaction was also a mixture of isotopologues and isotopomers as judged by a combination of ^{2}H NMR spectroscopy and mass spectrometry (LC-MS, ESI mode). Although dehydrogenation of the aryl substituents was markedly slower than in the intermolecular case, reversible cyclometallation still occurred at a similar rate for both the intra- and intermolecular [2+2] cycloadditions, leading to almost identical deuterium scrambling patterns on both the products and the recovered ligands.

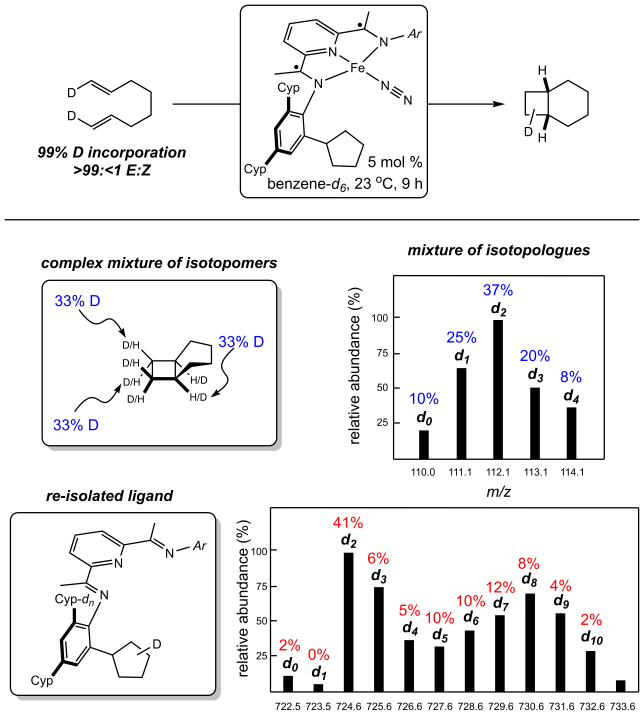

Figure 15. Iron-catalyzed [2+2] cycloaddition of 1,8-dideutero-*E,E*-1,7-octadiene and techniques to determine number of isotopologues and isotopomers. The mass spectrum histograms are representations of the originals, which can be found in the Supporting Information.

Reaction of other diene substrates was explored to evaluate whether ligand cyclometallation could be suppressed by increasing

the rate of [2+2] cycloaddition. In the presence of 5 mol % **(^{tric}PDI)Fe(N_2)**, the [2+2] cycloaddition of *N,N*-bis(3-deutero-*Z*-allyl)-4-fluoroaniline was complete within 2 hours at 23 °C, significantly faster than the cycloaddition of 1,7-octadiene (Figure 16). The degree of deuterium scrambling was also significantly reduced as only 19% of the total deuterium was incorporated at the substituted position of the cyclobutane ring. A 90:10 mixture of only two isotopomers was observed by ^{2}H NMR spectroscopy, significantly reduced from the complex mixture observed from the cycloaddition products of 1-deutero-*E*-1-octene and 1,8-dideutero-*E,E*-1,7-octadiene. As reported previously,[4a] the [2+2] cycloaddition of *N,N*-(3-deutero-*Z*-allyl)-*tert*-butylamine was complete in less than 5 minutes at 23 °C and the product was obtained as a single isotopomer and isotopologue. Due to the increased rate of reaction, cyclometallation was likely too slow to compete with cycloaddition and no scrambling was observed. Based on this data, it is likely that C(sp^3)–C(sp^3) reductive elimination occurs either by a concerted mechanism or a stepwise mechanism where the rate of radical recombination is significantly faster than the rate of C–C bond rotation.[36]

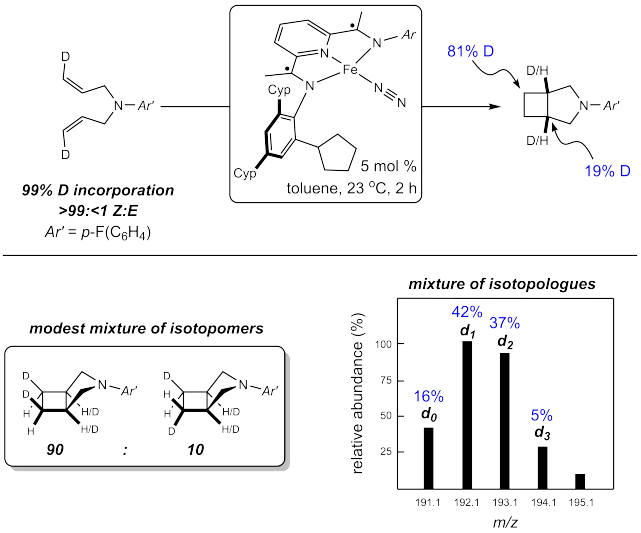

Figure 16. Iron-catalyzed [2+2] cycloaddition of *N,N*-bis(3-deutero-*Z*-allyl)-4-fluoroaniline and techniques to determine number of isotopologues and isotopomers. The mass spectrum histograms are representations of the originals, which can be found in the Supporting Information.

Computational studies on *C–C* bond forming processes in PDI iron-catalyzed cycloaddition reactions have been reported previously by Chen and co-workers[37] and we wish to address some of their findings. Our experimental results on the symmetry allowed, unimolecular reductive elimination of $S = 1$ PDI ferracyclopentanes are in line with lowest energy reaction coordinate obtained by Chen and co-workers for this pathway. The calculated transition state energy for the reductive elimination process studied by Chen and co-workers (24.4 kcal·mol^{-1}) is also nearly identical to the experimentally determined transition state energy of 24.5 kcal·mol^{-1} for reductive elimination of the *trans*-bicycle from **(^{dic}PDI)Fe(*trans*-bimetallacyclo[4.3.0]nonane)**, further corroborating both our group's and Chen's computational results on [2+2] alkene dimerization.

■ CONCLUSIONS

Comprehensive experimental and computational studies have been conducted to gain insight into the mechanism of both inter- and intramolecular iron-catalyzed [2+2] cycloadditions of alkenes and to determine similarities and differences between the two processes. For the iron-catalyzed [2+2] cycloaddition of 1-octene, a reaction first order in both iron precatalyst and alkene but inverse first order with respect to dinitrogen was observed. The coordinatively saturated iron alkene complex, **(^{tric}PDI)Fe(N_2)(η^2-1-octene)** was established as the catalyst resting state via a combination of infrared and freeze-quench ^{57}Fe Mössbauer spectroscopy. These observations support slow release and rate-determining association of the second alkene substrate to a four-coordinate (^{tric}PDI)Fe alkene complex. Because catalyst turnover to either **(^{tric}PDI)Fe(N_2)** or **(^{tric}PDI)Fe(η^2-alkene)** is possible, it is currently unknown whether the catalyst resting state is on- or off-cycle. Competing cyclometalation of the aryl substituents of the chelate resulted in catalyst deactivation and ultimately death, arising from dehydrogenation of a cyclopentyl group.

For the intramolecular [2+2] cycloaddition of 1,7-octadiene, *cis*-bicyclo[4.2.0]octane was produced in >98% conversion and 92:8 d.r. A reaction first order in iron precatalyst and zeroth order in α,ω-diene and dinitrogen was observed, distinct from the intermolecular case. The iron metallacycle, **(^{dic}PDI)Fe(bimetallacyclo[4.3.0]nonane)** was found to be the catalyst resting state and, in combination with ^{12}C/^{13}C KIE measurements, underwent rate determining, unimolecular reductive elimination to form the bicyclic alkane product. Unlike the intermolecular case, the catalytic cycle likely remains on the $S = 1$ spin surface, a consequence of the chelate effect and the higher binding affinity of 1,7-octadiene compared to dinitrogen and 1-octene. While the observed iron *trans*-bimetallacycle is lower in energy, the transition state for reductive elimination of the *cis*-metallacycle is lower in energy, leading to preferential formation of the *cis*-bicycle. In both inter- and intramolecular reactions, competing cyclometalation of the aryl-substituents complicated stereochemcial determination of the C–C bond-forming step. In cases where the intramolecular catalytic reaction was sufficiently rapid, deuterium labeling supported a concerted pathway for reductive elimination or rapid radical rebound faster than C–C bond rotation. Future work will focus on the application of these mechanistic findings to next generation iron cycloaddition catalysts with improved scope and activity.

ASSOCIATED CONTENT

The Supporting Information is available free of charge via the Internet at http://pubs.acs.org and contains additional experimental details, characterization data including NMR spectra, Mössbauer spectra, mass spectrometry, and computational details and data.

Crystallographic information for **(^{dic}PDI)Fe(*trans*-bimetallacyclo[4.3.0]nonane)**, **(^{iPr,TB}PDI)Fe(bimetallacyclo[4.3.0]nonane)** and **(Et-^{Me}PDI)Fe(η^2-allylbenzene)(N_2)** (CIF).

AUTHOR INFORMATION

Corresponding Author

* Email for P.J.C. pchirik@princeton.edu

ORCID

Matthew V. Joannou: 0000-0002-0079-7107

Paul J. Chirik: 0000-0001-8473-2898

Notes

The authors declare no competing financial interest.

ACKNOWLEDGMENT

We thank Firmenich SA for financial support.

REFERENCES

[1] (a) Namyslo, J. C.; Kaufmann, D. E. The Application of Cyclobutane Derivatives in Organic Synthesis. *Chem. Rev.* **2003**, *103*, 1485–1538. (b) *The Chemistry of Cyclobutanes, Parts 1-2*; Rappoport, Z., Ed.; Wiley & Sons Ltd: Weinheim, Germany, 2005.

[2] (a) Wang, M.; Lu, P. Catalytic Approaches to Assemble Cyclobutane Motifs in Natural Product Synthesis. *Organic Chemistry Frontiers* **2018**, *5*, 254–259. (b) Erman, M. B.; Kane, B. J. Chemistry Around Pinene and Pinane: A Facile Synthesis of Cyclobutanes and Oxatricyclo-Derivative of Pinane from Cis- and Trans-Pinanols. *Chemistry & Biodiversity* **2008**, *5*, 910–919. (c) Du, J.; Yoon, T. P. Crossed Intermolecular [2+2] Cycloadditions of Acyclic Enones via Visible Light Photocatalysis. *J. Am. Chem. Soc.* **2009**, *131*, 14604–14605. (d) Ischay, M. A.; Anzovino, M. E.; Du, J.; Yoon, T. P. Efficient Visible Light Photocatalysis of [2+2] Enone Cycloadditions. *J. Am. Chem. Soc.* **2008**, *130*, 12886–12887. (e) Wang, Y.-M.; Bruno, N. C.; Placeres, Á. L.; Zhu, S.; Buchwald, S. L. Enantioselective Synthesis of Carbo- and Heterocycles through a CuH-Catalyzed Hydroalkylation Approach. *J. Am. Chem. Soc.* **2015**, *137*, 10524–10527. (f) Poplata, S.; Tröster, A.; Zou, Y.-Q.; Bach, T. Recent Advances in the Synthesis of Cyclobutanes by Olefin [2 + 2] Photocycloaddition Reactions. *Chem. Rev.* **2016**, *116*, 9748–9815. (g) Ito, H.; Toyoda, T.; Sawamura, M. Stereospecific Synthesis of Cyclobutylboronates through Copper(I)-Catalyzed Reaction of Homoallylic Sulfonates and a Diboron Derivative. *J. Am. Chem. Soc.* **2010**, *132*, 5990–5992. (h) Conner, M. L.; Brown, M. K. Synthesis of 1,3-Substituted Cyclobutanes by Allenoate-Alkene [2 + 2] Cycloaddition. *J. Org. Chem.* **2016**, *81*, 8050–8060.

[3] Chirik, P. J. Carbon–Carbon Bond Formation in a Weak Ligand Field: Leveraging Open-Shell First-Row Transition-Metal Catalysts. *Angew. Chem. Int. Ed.* **2017**, *56*, 5170–5181.

[4] (a) Bouwkamp, M. W.; Bowman, A. C.; Lobkovsky, E.; Chirik, P. J. Iron-Catalyzed [2π + 2π] Cycloaddition of α,ω-Dienes: The Importance of Redox-Active Supporting Ligands. *J. Am. Chem. Soc.* **2006**, *128*, 13340–13341. (b) Schmidt, V. A.; Hoyt, J. M.; Margulieux, G. W.; Chirik, P. J. Cobalt-Catalyzed [2π + 2π] Cycloadditions of Alkenes: Scope, Mechanism, and Elucidation of Electronic Structure of Catalytic Intermediates. *J. Am. Chem. Soc.* **2015**, *137*, 7903–7914. (c) Hoyt, J. M.; Schmidt, V. A.; Tondreau, A. M.; Chirik, P. J. Iron-Catalyzed Intermolecular [2+2] Cycloadditions of Unactivated Alkenes. *Science* **2015**, *349*, 960–963.
(d) Russell, S. K.; Lobkovsky, E.; Chirik, P. J. Iron-Catalyzed Intermolecular [2π + 2π] Cycloaddition. *J. Am. Chem. Soc.* **2011**, *133*, 8858–8861.

[5] Hoyt, J. M.; Sylvester, K. T.; Semproni, S. P.; Chirik, P. J. Synthesis and Electronic Structure of Bis(Imino)Pyridine Iron Metallacyclic Intermediates in Iron-Catalyzed Cyclization Reactions. *J. Am. Chem. Soc.* **2013**, *135*, 4862–4877.

[6] (a) Scott, D. R.; Allison, J. B. Solvent Glasses for Low Temperature Spectroscopic Studies. *The Journal of Physical Chemistry* **1962**, *66*, 561–562. (b) Greenspan, H.; Fischer, E. Viscosity of Glass-Forming Solvent Mixtures at Low Temperatures. *The Journal of Physical Chemistry* **1965**, *69*, 2466–2469.

[7] N.N. Greenwood, T.C. Gibb, Mössbauer Spectroscopy, Springer Netherlands, Dordrecht, 1971.

[8] Bart, S. C.; Lobkovsky, E.; Chirik, P. J. Preparation and Molecular and Electronic Structures of Iron(0) Dinitrogen and Silane Complexes and Their Application to Catalytic Hydrogenation and Hydrosilation. *J. Am. Chem. Soc.* **2004**, *126*, 13794–13807.

[9] Stieber, S. C. E.; Milsmann, C.; Hoyt, J. M.; Turner, Z. R.; Finkelstein, K. D.; Wieghardt, K.; DeBeer, S.; Chirik, P. J. Bis(Imino)Pyridine Iron Dinitrogen Compounds Revisited: Differences in Electronic Structure Between Four- and Five-Coordinate Derivatives. *Inorg. Chem.* **2012**, *51*, 3770–3785.

[10] For the calculation of K_{eq}, it was assumed that the symmetric and antisymmetric N_2 stretches of **(^{tric}PDI)Fe(N_2)$_2$** are of equal intensity as is reported for (^{iPr}PDI)Fe(N_2)$_2$ (ref. 8).

[11] (a) Singleton, D. A.; Thomas, A. A. High-Precision Simultaneous Determination of Multiple Small Kinetic Isotope Effects at Natural Abundance. *J. Am. Chem. Soc.* **1995**, *117*, 9357–9358. (b) Frantz, D. E.; Singleton, D. A.; Snyder, J. P. ^{13}C Kinetic Isotope Effects for the Addition of Lithium Dibutylcuprate to Cyclohexenone. Reductive Elimination Is Rate-Determining. *J. Am. Chem. Soc.* **1997**, *119*, 3383–3384.

[12] Kennedy, C. R.; Zhong, H.; Macaulay, R. L.; Chirik, P. J. Regio- and Diastereoselective Iron-Catalyzed [4+4] Cycloaddition of 1,3-Dienes. *J. Am. Chem. Soc.* **2019**, *141*, 8557-8573

[13] If the reaction is mixed thoroughly before freezing to 77 K, a 50:50 mixture of **(^{tric}PDI)Fe(N_2)** and **(^{tric}PDI)Fe(N_2)(η^2-1-octene)** is observed in the zero-field ^{57}Fe Mössbauer spectrum. The precatalyst is not completely soluble in 1-octene, which is the likely source of this observation. The other quadrupole doublet observed in Figure 5 accounts for only 8% of the total iron content of the sample. It is currently unknown whether this signal corresponds to another iron species generated during the cycloaddition reaction or a small amount of decomposition formed during sample preparation.

[14] Bart, S. C.; Lobkovsky, E.; Bill, E.; Wieghardt, K.; Chirik, P. J. Neutral-Ligand Complexes of Bis(Imino)Pyridine Iron: Synthesis, Structure, and Spectroscopy. *Inorg. Chem.* **2007**, *46*, 7055–7063.

[15] Chirik, P. J. Preface: Forum on Redox-Active Ligands. *Inorg. Chem.* **2011**, *50*, 9737–9740.

[16] Because it was difficult to obtain crystals suitable for X-ray diffraction of **(^{tric}PDI)Fe(η^2-1-octene)(N_2)**, other olefins and PDI ligand combinations were tested to improve crystallinity of an olefin-N_2 complex. Several single crystals of **(Et-^{Me}PDI)Fe(η^2-allylbenzene)(N_2)** were obtained from **[(Et-^{Me}PDI)Fe(N_2)]$_2$(μ-N_2)** in a mixture of pentane and allylbenzene in a -35 °C freezer. Large amounts of this compound could not be isolated for thorough characterization, but the X-ray structure, which is of high quality, lends support for assignment of the Mössbauer spectrum in Figure 5 as well as starting points for DFT calculations (see Supporting Information for a depiction of the solid-state structure).

[17] Römelt, M.; Ye, S.; Neese, F. Calibration of Modern Density Functional Theory Methods for the Prediction of 57Fe Mössbauer Isomer Shifts: Meta-GGA and Double-Hybrid Functionals. *Inorg. Chem.* **2009**, *48*, 784–785.

[18] Trovitch, R. J.; Lobkovsky, E.; Chirik, P. J. Bis(Imino)Pyridine Iron Alkyls Containing β-Hydrogens: Synthesis, Evaluation of Kinetic Stability, and Decomposition Pathways Involving Chelate Participation. *J. Am. Chem. Soc.* **2008**, *130*, 11631–11640.

[19] DFT simulated ^{57}Fe Mössbauer parameters for both regioisomers of **(dehydro-^{tric}PDI)Fe(N_2)** matched those obtained experimentally and are presented in the Supporting Information. Additionally, while small amounts of the cyclobutane product are still being formed after 8 hours of reaction, the diminished signal for the catalyst resting state is likely obscured by the signal for **(dehydro-^{tric}PDI)Fe(N_2)**.

[20] P. Gütlich, E. Bill, A.X. Trautwein, Mössbauer Spectroscopy and Transition Metal Chemistry, Springer-Verlag, Berlin Heidelberg, 2011.

[21] Optimization of (^{dic}PDI)Fe(η^2-propylene)$_2$ in a BS(3,1), $S = 1$ configuration led to dissociation of one imine arm of the PDI ligand. This has been previously observed both experimentally and computationally in reference 5.

[22] Low spatial orbital overlap of this type has been calculated previously in PDI iron complexes, especially those with broken symmetry electronic configurations such as (PDI)Fe(N_2). See reference 9.

[23] (a) Hopmann, K. H. How Accurate is DFT for Iridium-Mediated Chemistry? *Organometallics* **2016**, *35*, 3795-3807. (b) Wodrich, M.D.; Corminboeuf, C.; Schreiner, P.R.; Fokin, A.A.; von Ragué Schleyer, P. How Accurate are DFT Treatments of Organic Energies. *Org. Lett.* **2007**, *9*, 1851-1854.

[24] The Fe-catalyzed [2+2] cycloaddition of 1,7-octadiene conducted at 4 atm N_2 reaches 50% conversion in 2.5 hours and complete conversion in 9 hours (identical to the 0 and 1 atm experiments), which further supports that the reaction is zeroth order in [N_2].

[25] (a) *Inorganic and Organometallic Reaction Mechanisms*. Atwood, J. D. Wiley-VCH Inc., 1997. (b) Blackmond, D. G. Reaction Progress Kinetic Analysis: A Powerful Methodology for Mechanistic Studies of Complex Catalytic Reactions. *Angew. Chem. Int. Ed.* **2005**, *44*, 4302–4320.

[26] Small quantities of 2,6-dicyclopentylaniline were initially purchased from Sigma-Aldrich but it has since been discontinued. ^{tric}PDI is more readily accessible due to its straightforward synthesis beginning with Friedel-Crafts tri-alkylation of benzene with cyclopentyl bromide.

[27] Bart, S. C.; Chłopek, K.; Bill, E.; Bouwkamp, M. W.; Lobkovsky, E.; Neese, F.; Wieghardt, K.; Chirik, P. J. Electronic Structure of Bis(Imino)Pyridine Iron Dichloride, Monochloride, and Neutral Ligand Complexes: A Combined Structural, Spectroscopic, and Computational Study. *J. Am. Chem. Soc.* **2006**, *128*, 13901–13912.

[28] Grubbs, R. H.; Miyashita, A. Preparation and Isomerization Reactions of 2-Nickelahydrindanes. *Journal of Organometallic Chemistry* **1978**, *161*, 371–380.

[29] *Solution NMR of Paramagnetic Molecules*. Bertini, I.; Luchinat, C.; Parigi, G., Ed.; Elsevier Science: Amsterdam, The Netherlands, 2001.

[30] Because the exact process accounting for the isomerization from *trans*- to *cis*-bimetallcycle is unknown (and likely involves several distinct steps), either a primary or inverse ^{13}C KIE could be observed at all cyclobutane carbons of the product. Although, the magnitude is likely to be small as the effect will be averaged over 4 cyclobutane carbons.

[31] *Modern Physical Organic Chemistry*. Anslyn, E. V.; Dougherty, D. A. University Science Books, 2007.

[32] *Advanced Organic Chemistry, Part A: Structure and Mechanisms*. Carey, F. A.; Sundberg, R. J. Springer Science and Business Media, LLC, 2007.

[33] The *cis*-product is also 5 kcal·mol^{-1} lower in energy than the *trans*. While the relative stability of the products does not dictate the distribution of products in a Curtin-Hammett scenario, it is still worthwhile to mention. This calculation also accurately matches the energy difference between a twist-boat and boat cyclohexane conformation (4.5 kcal·mol^{-1}) (cf. reference 27)

[34] Lau, W.; Huffman, J. C.; Kochi, J. K. Electrochemical Oxidation-Reduction of Organometallic Complexes. Effect of the Oxidation State on the Pathways for Reductive Elimination of Dialkyliron Complexes. *Organometallics* **1982**, *1*, 155–169.

[35] After 18 hours at 23 °C, small amounts of isomerized 1-octene were also observed.

[36] The barrier for C–C bond rotation about ethane has been calculated to be 2.9 kcal·mol^{-1}, while that for ethyl radical is 0.8 kcal·mol^{-1}. This suggests that the rate of radical recombination in the stepwise mechanism could be $\geq 10^{10}$ s^{-1}, which would likely be kinetically indistinguishable from a concerted reductive elimination mechanism. (a) Pacansky, J.; Coufal, H. On the Barrier for Rotation about the C–C Bond of the Ethyl Radical. *The Journal of Chemical Physics* **1980**, *72*, 5285–5286. (b) Edidin, M. A.; Ratto, T. V.; Longo, M. L.; Sturtevant, J. M.; Sandhoff, K.; Simons, K.; Vogel, H.; Nelson, W. J. Ultrafast Carbon-Carbon Single-Bond Rotational Isomerization in Room-Temperature Solution. *Science* **2006**, *313*, 1951-1954.

[37] Hu, L.; Chen, H. Substrate-Dependent Two-State Reactivity in Iron-Catalyzed Alkene [2+2] Cycloaddition Reactions. *J. Am. Chem. Soc.* **2017**, *139*, 15564–15567.

For Table of Contents Use